ENHANCED LOWER HYBRID HEATING DUE TO FREQUENCY MODULATION

Spilios Riyopoulos
Institute for Fusion Studies
The University of Texas
Austin, Texas 78712

Abstract

The effect of frequency modulation during stochastic ion heating induced by lower hybrid waves is examined. The modulation occurs either in the ion cyclotron frequency due to the variation of the magnetic field in toroidal devices, or it can be externally imposed on the frquency of the lower hybrid waves. It has already been observed numerically [Phys. Fluids 27, 184(1984)] that a small variation in the ion cyclotron frequency can induce velocity diffusion for wave amplitude well below the stochasticity threshold in a uniform magnetic field. Here a detailed study reveals that to the lowest order in the small parameters, the modulational effects can be incorporated in a two-dimensional Hamiltonian. This allows the derivation of the new stochasticity thresholds. It is found that a small amount of modulation, $\frac{\Delta\omega}{\omega} \lesssim 1\%$, produces an order of magnitude reduction in the stochasticity threshold relative to the constant frequency case. The stochastic regime in velocity space also grows in size, resulting in a considerable increase of the number of heated particles in the case of devices with modest aspect ratio. Both ion cyclotron and wave frequency modulation lead to similar results. The modulation of the wave frequency offers the ability to control and optimize the modulation parameters and is proposed as a method to enhance RF heating.

I. INTRODUCTION

The interaction of a charged particle with a coherent electrostatic wave propagating perpendicularly to a static magnetic field has been extensively studied in a number of papers. Karney[1] has considered this problem for the case of a uniform $\underset{\sim}{B}$-field. He has shown that under certain conditions the equations of motion of the particle are well-approximated by a discrete two-dimensional map of the form

$$u_{j+1} = u_j + 2\pi\delta - 2\pi A \cos v_j$$
$$v_{j+1} = v_j + 2\pi\delta + 2\pi A \cos u_{j+1} \tag{1}$$

with

$$u_j = \vartheta_j - \rho_j \quad , \quad v_j = \vartheta_j + \rho_j$$

where ρ_j and ϑ_j specify the particle speed perpendicular to $\underset{\sim}{B}$ and its gyrophase. The index j signifies that these quantities are evaluated at the j-th cyclotron period. The quantities A and δ are parameters of the system; A is the normalized wave amplitude and δ the normalized wave frequency; $\delta = \omega/\omega_c$ mod 1, where ω and ω_c are the wave frequency and the particle gyrofrequency. Karney finds that when A exceeds a critical value, $A_s \sim 0.25$, widespread diffusive behavior of the particle energy results. Thus, if the amplitude of the wave is large enough, energy transfer from the wave to the particles becomes possible and heating of the plasma results.[1,2] In particular, this picture has

been invoked with reference to ion heating in lower hybrid heating experiments.[3]

Karney's map was modified in Ref. 4 to include the effect of the nonuniformity in the magnetic field, a familiar situation in many cases of interest. As the magnetic field strength changes, ion cylcotron frequency ω_c changes as well and the frequency mismatch δ, defined in the previous paragraph, is modulated in time instead of being a constant. It was argued that for sinusoidally varying magnetic field strength and free streaming particles along the magnetic lines

$$\underset{\sim}{B} = B_0(1 + \varepsilon \sin kz)^{-1}\,\hat{z}, \quad v_z = \text{const.}\ ,$$

the autonomous map (1) valid in the uniform $\underset{\sim}{B}$-field case evolves into a similar nonautonomous map, by replacing δ = const. with

$$\delta_j = \delta_0 + \varepsilon\nu \sin 2\pi j\Omega\ ,\ \Omega = kv_z/\omega_c\ , \tag{2}$$

an explicit function of time $t_j = 2\pi j$. Numerical results[4] obtained by iterating Eq. (1) with modulated δ_j, Eq. (2), showed that relatively small size ripple in the magnetic field ($\varepsilon \lesssim 1\%$) can completely change the behavior of the system, inducing diffusion of the particle velocity for values of the wave amplitude A much lower than the homogeneous magnetic field stochasticity threshold A_s. The observed thresholds for fast diffusion were much lower than the uniform field stochasticity threshold A_s, while slow diffusion persisted for very small wave amplitudes. An analytic derivation of the fast diffusion thresholds was not possible through the framework of Ref. 4, and remains to be considered. The effect of the inhomogeneity on the boundaries of the

stochastic regime in velocity space also needs to be examined since, after all, it will determine the percentage of particles that absorb energy from the wave. Finally, the approximations made during the introduction of the nonautonomous map, considering the variation of $|\underset{\sim}{B}|$ along magnetic lines as the main effect (i.e., ignoring perpendicular gradients) and assuming the ions free streaming in the same direction, need to be justified in a more systematic way. Note that the time variation of the mismatch δ_j between the cyclotron frequency ω_c and the wave frequency ω can be produced by the modulation of either one of the above two characteristic frequencies. Although variation of ω_c is inherent in toroidal devices due to variation of the magnetic field strength, it can be advantageous to externally modulate the wave frequency ω, offering the possibility of optimizing the modulation parameters.

In this paper the emphasis will be given initially to the detailed study of the case when the cyclotron frequency ω_c is modulated due to toroidal effects. The Hamiltonian formalism will be used to show that, for small size ripple ε in the magnetic field, the system behaves as a two-dimensional system and this behavior determines the fast scale diffusion. Proper action angle variables will be introduced for the study of the surfaces of section and the transition to chaos. Lower thresholds compared to the uniform magnetic field case are expected as the modulation frequency Ω introduces a new family of resonances in the system. This indeed turns out to be the case, when an appropriate condition is satisfied. Turning back to the map representation, this condition simply means that δ_j can go through one of the principal resonances $\delta=0$ or $\delta=1/2$ of the uniform field case. The nonautonomous

map will be derived from the Hamiltonian of the system, justifying the use of Eqs. (1) and (2) to approximate the particle motion. Next the attention will be turned to the case when the wave frequency ω is modulated externally while ω_c remains constant. It will be proved that this process is physically equivalent to that of the ω_c modulation, leading to similar conclusions. The picture will be completed with the study of the enlargement of the stochastic regime in velocity space due to the modulation, producing enhanced power absorption from the wave.

The outline of the remainder of this paper is as follows. In Sec. II a large aspect ratio, slab geometry model is used to write the Hamiltonian of a particle in a tokamak static field under the influence of an electrostatic wave propagating perpendicularly to the field lines. Keeping only first order terms in the perturbation parameters reduces the system into a two-dimensional one. Then the equations of motion in the rippled magnetic field are derived. Resonant approximation is used to define the new action-angle variables. In Sec. III the motion on a surface of section in the phase space is examined for different parameter values. Existence of invariant KAM surfaces for wave amplitudes below some threshold is verified by direct numerical integration of the equations of motion. The island overlapping technique is applied in Sec. IV for the evaluation of the new large scale chaos threshold, and the process is repeated for the higher order islands. It is found that the maximum reduction of one or two orders of magnitude in the wave amplitude threshold occurs for such parameters ε,ν that allow δ_j to go through the main resonances (δ=0 or δ=1/2), of the uniform field case.

In Sec. V the nonautonomous map, Eqs. (1) and (2), is derived from the Hamiltonian of Sec. II. The addtional validity condition to these obtained by Karney for the uniform field case is that the modulation frequency Ω is slow enough for δ_j to be considered constant during one gyroperiod. The quantities ρ_j and ϑ_j are now computed at the end of the j-th "reduced" gyroperiod, introduced through the transformations of Sec. II. In addition, ρ signifies the square root of the magnetic moment $\mu^{1/2}$ rather than perpendicular velocity. Since in normalized units $v_\perp \cong (1-\varepsilon)^{1/2}\mu^{1/2}$, the diffusion coefficients derived elsewhere[4] are still valid for diffusion in velocity space for ε small. In the same section the apparent contradiction between the dimensionality of the nonautonomous map and the time autonomous Hamiltonian from which it is derived will be resolved. To be more specific, the explicit time dependence in Eq. (2) is not generic but imposed due to an approximation. The fast diffusion above a certain threshold in A, observed in Ref. 4, is connected with the destruction of the invariant KAM surfaces, shown in Sec. III. The persisting extremely slow diffusion below this threshold occurs due to the higher than 2 dimensionality of the map.[5]

In Sec. VI equivalence is established between the modulation in frequency mismatch δ due to the $\underset{\sim}{B}$-field nonuniformity, and the modulation of δ in a uniform $\underset{\sim}{B}$-field due to an external variation of the driving wave frequency. The new stochasticity threshold is computed numerically as a function of the modulation parameters and the results are in good agreement with the theoretical predictions of Sec. IV. Frequency modulation in the LH waves is proposed as a method to lower the wave amplitude threshold for effective RF heating.

In Sec. VII the study is extended to include the case of a big size ripple in the magnetic field, connected with the heating of compact tori. When ε is a modest fraction of one, the small parameter expansion of Sec. II fails, and the full set of equations of motion in three dimensions must be solved simultaneously. Numerical integration shows that the velocity threshold for stochastic ion heating is lowered considerably, and thus heating can become more efficient, as the population of the responding particles increases exponentially with decreasing velocity. Section VIII is the conclusion.

II. DERIVATION OF THE HAMILTONIAN

Here a Hamiltonian will be derived for a particle gyrating in the magnetic field of a tokamak, including the effects of the variation of $|\underset{\sim}{B}|$ along the magnetic lines. In the large aspect limit and using rectangular coordinates with z along the field lines and y along the direction of propagation of the electrostatic wave,

$$\underset{\sim}{E} = \hat{y}E_0\cos(k_\perp y-\omega t) \ ,$$

$\underset{\sim}{B}$ can be modeled by

$$(B_x,B_y,B_z) = B_0(0,\ \varepsilon\cos k'z\sin k'y,\ 1 - \varepsilon\sin k'z\cos k'y) \ ,$$

where

ε = inverse aspect ratio = r/R ,

$k' = (Rq)^{-1}$,

q = safety factor $\gtrsim 1$,

r = minor and R = major radius of the torus ,

and the condition $\nabla \cdot \mathbf{B} = 0$ is satisfied. $\mathbf{B}$ can be derived from a vector potential $\mathbf{A}$ through $\mathbf{B} = \nabla \times \mathbf{A}$ with $\mathbf{A}$ given by

$$\mathbf{A} = (A_x, 0, 0) = -B_0(y - \varepsilon/k' \sin k'z \sin k'y,\ 0,\ 0) \ .$$

Larmor radius ρ_i is considered small compared with the magnetic ripple wavelength $2\pi/k'$ but large compared to the electrostatic wavelength $2\pi/k_\perp$ according to

$$k'\rho_i \ll 1 \ll k_\perp \rho_i \ .$$

This situation is different from the one examined by Gell and Nakach;[6] they considered the finite Larmor radius effects of a magnetic gradient perpendicular to both the field lines and the direction of propagation of the wave with constant $\mathbf{B}$ along z, while here finite Larmor radius effects in association with the perpendicular gradient are shown to be less important, and the dynamics is determined by the variation of the magnetic field strength along the field lines. Since the motion perpendicular to $\mathbf{B}$ is to remain bounded for long periods, $k'y \sim k'\rho_i \ll 1$, and an expansion of the sin $k'y$ term in the vector potential yields

$$A_x \cong -yB_0(1-\varepsilon\sin k'z) + 0[\frac{\varepsilon}{k'}(k'\rho_i)^3] \ .$$

The Hamiltonian H is given by

$$H = H_0 - \frac{|e|E_0}{k_\perp}\sin(k_\perp y-\omega t) \ ,$$

$$H_0 = \frac{1}{2m}\left\{[P_x + m\omega_{co}y(1-\varepsilon\sin kz)]^2 + P_y^2 + P_z^2\right\} \ ,$$

where $\omega_{co} = eB_0/m_i c$. Renormalizing lengths to $k_\perp^{-1}$ and time to ω_{co}^{-1}, we obtain H in a dimensionless form

$$H = \frac{1}{2}\left\{y^2(1-\varepsilon\sin\kappa z)^2 + P_y^2 + P_z^2\right\} - \alpha\sin(y-\nu t) \qquad (3a)$$

where

$$\alpha = \frac{|e|E_0k_\perp}{m\omega_{co}^2} \ , \ \nu = \omega/\omega_{co} \ , \ \kappa = k'/k_\perp \ .$$

and

$$\dot{x} = y(1-\varepsilon\sin\kappa z) \ .$$

The purpose now is to introduce an approximate Hamiltonian linear in the small parameters ε, κ, $\alpha\sim O(\lambda)$ with $\lambda<<1$. This is done by applying successively the canonical transformations

$$q_y = (1-\varepsilon\sin\kappa z)^{1/2} y \ , \qquad Q_y = (1-\varepsilon\sin\kappa z)^{-1/2} P_y \ ,$$

$$q_z = z \ , \qquad Q_z = P_z - \frac{\varepsilon\kappa\cos\kappa z}{1-\varepsilon\sin\kappa z} P_y y \ , \tag{3b}$$

and

$$q_y = (2I_1)^{1/2} \sin\vartheta_1 \ ,$$

$$Q_y = (2I_1)^{1/2} \cos\vartheta_1 \ , \tag{3c}$$

and discarding terms of order λ^2 or higher. The mathematical details of the derivation are given in Appendix A. The new approximate Hamiltonian is

$$K(\vartheta_1, z, I_1, P_z; t) \equiv (1-\varepsilon\sin\kappa z) I_1 + \frac{1}{2} P_z^2 - \alpha\sin[(2I_1)^{1/2}\sin\vartheta_1 - \nu t] \ . \tag{4}$$

The energy of the particle in the magnetic field is given by

$$K_0 = (1-\varepsilon\sin\kappa z) I_1 + \frac{1}{2} P_z^2 \ ,$$

Here I_1 is the normalized magnetic moment

$$I_1 = \left(\frac{m\omega_{co}^2}{k_\perp^2 B_0}\right)^{-1} \left[\frac{\frac{1}{2} m v_\perp^2}{B_0(1-\varepsilon\sin\kappa z)} = \mu\right] \ ,$$

and ϑ_1 is the reduced gyroangle expressed through Eqs. (3b) and (3c) as

$$\vartheta_1 = \tan^{-1}\{(1-\varepsilon\sin\kappa z)\,\frac{y}{P_y}\} \ .$$

In the absence of the wave interaction given by the term $\alpha\,\sin[(2I_1)^{1/2}\sin\vartheta_1-\nu t]$ in Eq. (4) the magnetic moment I_1 is an invariant of the motion according to

$$\dot{I}_1 = \alpha\,\frac{\partial K_1}{\partial\vartheta_1}\ , \qquad \dot{\vartheta}_1 = (1-\varepsilon\sin\kappa z)\ , \tag{5a}$$

$$\dot{P}_z = I_1\varepsilon\kappa\cos\kappa z\ , \qquad \dot{z} = P_z\ . \tag{5b}$$

One can now obtain the first-order solutions $z(t)$, $P_z(t)$ from Eqs. (5b) applying perturbation theory. The details of the derivation are given again in Appendix A. Replacing z and P_z in (4) with their approximate solutions $z(t)$ and $P_z(t)$ leads to the new one-dimensional, time-dependent Hamiltonian

$$K \cong (1-\varepsilon\sin\Omega t)I_1 - \alpha\,\sin[(2I_1)^{1/2}\sin\vartheta_1-\nu t]\ . \tag{6}$$

Finally, introducing $(-t,E)$ as a pair of canonical variables, where E is the total energy, we obtain the following two-dimensional, autonomous Hamiltonian

$$K = [1-\varepsilon\sin(\frac{\Omega}{\nu}\,\vartheta_2)]I_1 + \nu I_2 - \alpha\,\sin[(2I_1)^{1/2}\sin\vartheta_1-\vartheta_2]\ . \tag{7}$$

where

$$\vartheta_2 = \nu t \ , \ I_2 = -\nu^{-1}E \ .$$

It represents two harmonic oscillators, coupled through the nonlinear wave term, with one of their fundamental frequencies being slowly modulated according to $1 - \varepsilon\sin(\frac{\Omega}{\nu}\vartheta_2)$. In the limit of either $\varepsilon\to 0$, or $\Omega\to 0$,

$$K \to I_1 + \nu I_2 - \alpha \sin[(2I_1)^{1/2}\sin\vartheta_1 - \vartheta_2] \ ,$$

while

$$I_1 = \{\frac{1}{2}\ [\frac{P_y^2}{1-\varepsilon\sin\Omega t} + y^2(1-\varepsilon\sin\Omega t)]\}^{1/2} \to \{\frac{p_y^2+y^2}{2}\}^{1/2}$$

and we recover the uniform $\underset{\sim}{B}$-field results, discussed in Ref. 1.

The equations of motion, derived from (5) are expressed in the velocity-like variables Q_y, q_y, defined through Eq. (3b) and (3c) as

$$\dot{q}_y = Q_y(1-\varepsilon\sin\Omega t) \ ,$$

$$\dot{Q}_y = -(1-\varepsilon\sin\Omega t)q_y + \alpha\cos(q_y-\nu t) \ . \tag{8a}$$

The above Eqs. (8a) are combined into

$$\ddot{q}_y + \frac{\varepsilon\Omega\cos\Omega t}{1-\varepsilon\sin\Omega t}\ \dot{q}_y + (1-\varepsilon\sin\Omega t)^2 q_y = \alpha\ \cos(q_y-\nu t) \ . \tag{8b}$$

Note that if one neglects the second order term $\propto \varepsilon\Omega\dot{q}_y$, the LHS of Eq. (8b) is the equation of motion for an harmonic oscillator with a

time modulated characteristic frequency. As we should expect, at the limit $\varepsilon \to 0$ or $\Omega \to 0$ both $(Q_y, q_y) \to (P_y, y)$ and also Eq. (8b) $\to \ddot{y}+y = \alpha\cos(y-\nu t)$, i.e., we recover the uniform $\underset{\sim}{B}$-field results.

Expression (7) for the Hamiltonian will be used later in Sec. V for the derivation of the nonautonomous map (1) used to model the behavior in a nonuniform $\underset{\sim}{B}$-field, thus establishing the validity of the finite difference approach. We proceed now in order to define proper action-angle variables. Hamiltonian (7) can be written as

$$K = K_0 + K_1 \ ,$$

where K_0 is the integrable part

$$K_0 = \left(1-\varepsilon\sin\frac{\Omega}{\nu}\vartheta_2\right)I_1 + \nu I_2 \ ,$$

since it possesses a second integral of motion, $I_1 = C$. Therefore, the angle dependence in K_0 can be eliminated by introducing proper action-angle variables such that, to zeroth order in α, $\dot{\tilde{I}}_1 = \dot{\tilde{I}}_2 = 0$, $\dot{\tilde{\vartheta}}_1 = \text{const.}$, $\dot{\tilde{\vartheta}}_2 = \text{const.}$, This is done using the generating function

$$\tilde{F}[\tilde{I}_1, \tilde{I}_2, \vartheta_1, \vartheta_2] \equiv \tilde{I}_1\vartheta_1 + \nu^{-1}\left[\tilde{I}_2\vartheta_2 - \frac{\varepsilon\nu}{\Omega}\cos\left(\frac{\Omega}{\nu}\vartheta_2\right)\tilde{I}_1\right] \ .$$

Then

$$\tilde{I}_2 = \nu I_2 - \varepsilon I_1 \sin \frac{\Omega}{\nu} \vartheta_2 \ , \qquad \vartheta_2 = \nu \tilde{\vartheta}_2 \ ,$$

$$\tilde{I}_1 = I_1 \ , \qquad \vartheta_1 = \tilde{\vartheta}_1 + \frac{\varepsilon}{\Omega} \cos \Omega \tilde{\vartheta}_2 \ , \tag{9a}$$

and K is transformed into $\tilde{K} = \tilde{K}_0 + \tilde{K}_1$,

$$\tilde{K}_0 = \tilde{I}_1 + \tilde{I}_2 \ ,$$

$$\tilde{K}_1 = -\alpha \sin \left[(2\tilde{I}_1)^{1/2} \sin(\tilde{\vartheta}_1 + \frac{\varepsilon}{\Omega} \cos\Omega\tilde{\vartheta}_2) - \nu\tilde{\vartheta}_2 \right] \ .$$

Expansion of the perturbation in a series yields

$$\tilde{K} = \tilde{I}_1 + \tilde{I}_2 - \alpha \sum_{m,\ell} J_m[(2\tilde{I}_1)^{1/2}] J_\ell[\frac{\varepsilon m}{\Omega}] \times \sin[m\tilde{\vartheta}_1 - (\nu - \ell\Omega)\tilde{\vartheta}_2 + \frac{\ell\pi}{2}] \ . \tag{9b}$$

Hamiltonian $\tilde{K} \equiv \tilde{K}_0 + \tilde{K}_1$ is generally nonperiodic in $\tilde{\vartheta}_2$ unless ν and Ω are commesurable: $\nu/\Omega = p/q$, p,q integers. If, however, ν is close enough to a resonance we can reduce $\tilde{K}$ to an approximate form periodic in $\tilde{\vartheta}_2$ by keeping the dominant terms in the perturbation, i.e., terms with the phase varying slowly with time. Observing that to zeroth order $\dot{\tilde{\vartheta}}_1 = \dot{\tilde{\vartheta}}_2 = 1$, the closest to resonance terms in the expansion (9b) involve combinations of (m,ℓ) that satisfy

$$|\Delta(m,\ell)| < \Omega \quad \text{with} \quad \Delta(m,\ell) \equiv \nu - m - \ell\Omega \ .$$

Given that $M = \mathrm{Int}(\nu)$, $L = \mathrm{Int}(\frac{\nu-M}{\Omega})$, all the (m,ℓ) combinations that satisfy the above can be expressed as either

$$(M\pm s,\ L\mp sq) \quad \text{or} \quad (M\pm s,\ (L+1)\mp sq)$$

with $s=0,1,2,\ldots$ and $q = \mathrm{Int}(\frac{1}{\Omega})$. When $\alpha < \Omega$, according to the standard guidelines of Lee transforms (Deprit[7-8]), an infinitesimal transformation is possible that kills all other terms in the expanded Hamiltonian Eq. (9b), except the two closest to resonance families of terms. This is done by introducing

$$\hat{I}_1 = \tilde{I}_1 - \alpha \sum_{\substack{m \\ m\neq M\pm s}} \sum_{\substack{\ell \\ \ell\neq L\mp sq}} \frac{mJ_m(r)J_\ell(\frac{\varepsilon m}{\Omega})}{m-(\nu-\ell\Omega)} \sin[m\hat{\vartheta}_1 - (\nu-\ell\Omega)\hat{\vartheta}_2 + \frac{\ell\pi}{2})$$

$$\hat{I}_2 = \tilde{I}_1 + \alpha \sum_{\substack{m \\ m\neq M\pm s}} \sum_{\substack{\ell \\ \ell\neq L\mp sq}} \frac{(\nu-\ell\Omega)J_m(r)J_\ell(\frac{\varepsilon m}{\Omega})}{m-(\nu-\ell\Omega)} \sin(m\hat{\vartheta}_1 - (\nu-\ell\Omega)\hat{\vartheta}_2 + \frac{\ell\pi}{2}]$$

$$\tilde{\vartheta}_1 = \hat{\vartheta}_1 + \alpha \sum_{\substack{m \\ m\neq M\pm s}} \sum_{\substack{\ell \\ \ell\neq L\mp sq}} \frac{J_m(r)J_\ell(\frac{\varepsilon m}{\Omega})}{m-(\nu-\ell\Omega)} \cos[m\hat{\vartheta}_1 - (\nu-\ell\Omega)\hat{\vartheta}_2 + \frac{\ell\pi}{2}]$$

$$\tilde{\vartheta}_2 = \hat{\vartheta}_2 \ .$$

The above transformation changes the values of the variables very slightly; one finds, keeping the most important terms with (m,ℓ) in the vicinity of (M,L), that

$$\frac{\tilde{I}_1-\hat{I}_1}{\tilde{I}_1} \sim \frac{\alpha}{\Omega}\frac{M}{r^{5/2}} \quad , \quad r \gtrsim M >> 1 \ ,$$

and so to avoid further complication in the notation, one may take $\hat{I}_1 \cong \tilde{I}_1$, $\hat{\vartheta}_1 \cong \tilde{\vartheta}_1$ etc. The amplitudes corresponding to the surviving terms in the perturbation are given by

$$\alpha J_{M\pm s}(r) J_{L\mp sq}(x_{M\pm s})$$

where

$$r = \left(2\tilde{I}_1\right)^{1/2} \quad , \quad x_{M\pm s} = \frac{\varepsilon(M\pm s)}{\Omega} \ .$$

For Ω small q is large and one can ignore terms with $s\neq 0$. The new transformed $\tilde{K}$ is given by

$$\begin{aligned}\tilde{K} = \tilde{I}_1 + \tilde{I}_2 &- \alpha J_M(r) J_L\left(\frac{\varepsilon M}{\Omega}\right)\sin\left[M\tilde{\vartheta}_1 - (\nu-L\Omega)\tilde{\vartheta}_2 + \frac{L\pi}{2}\right] \\ &- \alpha J_M(r) J_{L+1}\left(\frac{\varepsilon M}{\Omega}\right)\sin\left[M\tilde{\vartheta}_1 - (\nu-(L+1)\Omega)\tilde{\vartheta}_2 + \frac{(L+1)\pi}{2}\right] \\ &+ O(\alpha^2) \ .\end{aligned} \tag{10}$$

One can assume that ν is much closer to the (M,L) than to (M,L+1) resonance, expressed by the condition

$$|\Delta(M,L)| << |\Delta(M,L+1)|$$

Keeping only the (M,L) resonant term in $\tilde{K}$ and performing a final transformation

$$\vartheta_2' = (\nu - L\Omega)\tilde{\vartheta}_2 \ , \qquad \tilde{I}_2 = (\nu - L\Omega) I_2' \ ,$$

$$\vartheta_1' = \tilde{\vartheta}_1 \ , \qquad \tilde{I}_1 = I_1' \ , \tag{11}$$

yields

$$K' = I_1' + (\nu - L\Omega) I_2' - \alpha' J_M((2I_1')^{1/2}) \sin[M\vartheta_1' - \vartheta_2' + \frac{L\pi}{2}] \ . \tag{12}$$

The structure of the above Hamiltonian is identical with that of the resonant Hamiltonian in the uniform $\underset{\sim}{B}$-field case,

$$K = I_1 + \nu I_2 - \alpha \ J_M[(2I_1)^{1/2}] \sin[M\vartheta_1 - \vartheta_2] \ ,$$

with

$$\begin{aligned} &\nu \ \text{ replaced by } \ \nu' \equiv \nu - L\Omega \ , \\ &\text{frequency mismatch } \delta \equiv \nu - M \text{ replaced by } \Delta \equiv \nu - L\Omega - M \ , \\ &\alpha \ \text{ replaced by } \ \alpha' \equiv \alpha \ J_L(\frac{\varepsilon M}{\Omega}) \ . \end{aligned} \tag{13}$$

The resonant amplitude α' is significant as long as $J_L(\frac{\varepsilon M}{\Omega})$ remains finite, hence the condition $\frac{\varepsilon M}{\Omega} \gtrsim L$ must hold. Physical interpretation of the above will be given in the next section. In the special case

when $\frac{\varepsilon M}{\Omega}$ approaches a zero x_n of $J_L(x)$, the next closest to resonance term, namely $J_{L+1}(\frac{\varepsilon M}{\Omega})$, must be kept in (10), and the same procedure as in Eqs. (11), (12) is repeated.

III. SURFACES OF SECTION

Hamiltonian Eq. (9b), or the resonant part of it, Eq. (11) are two-dimensional. Existence of invariant KAM surfaces[9] is expected, bounding the motion in phase space when the perturbation size α is below some threshold. In case when ν is close to a resonance, the proper action-angle variables can be chosen, as in Sec. II, so that the coherent periodic structure of the phase space in the nonstochastic case is revealed. The surfaces of section[10] are constructed by numerically integrating Eq. (8a) and then recording the values of either (Q_y, q_y) or (I_1', ϑ_1') every time the particle trajectory crosses the plane $\vartheta_2' = 2\pi$. Figures (1a) and (1b) show such surfaces for $\alpha = 0.0498$, $\varepsilon = 0.0055$, $\nu = 20.10023$. Figure (1a) clearly shows the bounded character of the motion when α is small, as particles are confined in a bounded regime in the Q_y, q_y plane. To see the periodic structure, we have to switch into the action-angle variables I_1', ϑ_1' obtained from Q_y, q_y through the successive transformations Eqs. (3b), (9a), (11) yielding

$$I_1' = \frac{1}{2}\left(Q_y^2 + q_y^2\right) ,$$

$$\vartheta_1' = \tan^{-1}(q_y/Q_y) - \frac{\varepsilon \cos\Omega t}{\Omega} .$$

Figure (1b) shows periodic coherent behavior demonstrating that although Hamiltonian (9b) is not exactly periodic in ϑ_2', the behavior of the system is dominated by the resonant part of (9b) Hamiltonian (12), which is periodic in ϑ_2'. Half of the total number of the stability islands are actually plotted, due to the initial conditions. Although the new frequency Ω, introduced through the modulation of the magnetic field strength, is small, it produces large changes in the behavior of the system. It adds new resonances and at the same time it lowers the threshold in the perturbation amplitude α for the appearance in phase space of the stability islands that correspond to each resonance. This can be seen by comparing Figs. 2 and 3, the first representing motion in a rippled and the second in a uniform (ε=0) magnetic field. Every other parameter being the same, islands appear only in (2b) where the modulation has been turned on.

The set of resonant values for ν becomes denser as nearby first order resonances (M,L) and (M,L+1), occuring whenever the new frequency mismatch becomes zero, i.e.,

$$|\Delta(M,L)| \equiv |\nu - M - L\Omega| \underset{\sim}{=} 0 \ ,$$

are separated by $\delta\nu = \Omega << 1$, while in the uniform $\underset{\sim}{B}$-field case we have $\delta\nu$=1 between successive resonances. For example, in Figs. 2 and 4 we have two different chains of islands corresponding to resonant values of ν = 20.10 and ν = 20.09 respectively. In addition, when Δ is not exactly 0, the threshold in α for the emergence of a stability islands chain is proportional to Δ, (see Sec. IV) which satisfies

$$\Delta \sim O(\Omega) << \delta \sim O(1) \ .$$

Large scale chaos results through the formation and overlapping of islands in phase space,[11,12,13] so both of the modulation effects tend to lower the threshold for stochasticity.

IV. NEW STOCHASTICITY THRESHOLD

IVA. First Order Islands

To illustrate how island chains appear for lower values of α due to the modulation Ω, Hamiltonian $K'(I_1', I_2', \vartheta_1', \vartheta_2')$ is reduced to a two-dimensional form that describes the motion on a given surface of section. First notice that K' possesses one more integral of motion:

$$I' = MI_2' + I_1' = \text{const.}$$

Letting $MI_\psi = I_1'$, $I_\varphi = I'$, $\psi = M\vartheta_1' - \vartheta_2'$, $\varphi = \vartheta_2'$ be the new canonical variables, the trajectories on a given surface of section $\vartheta_2' = C$ are derived from the Hamiltonian

$$h = K' - (\nu - L\Omega) I_\varphi$$

or

$$h = (M + L\Omega - \nu) I_\psi - \alpha J_M(r) J_L\left(\frac{\varepsilon M}{\Omega}\right) \sin\left(\psi + \frac{L\pi}{2}\right) \ . \tag{14}$$

The stationary elliptic points at the surface of section are given by

$$\psi_k = \frac{2k+1}{2}\pi - \frac{L}{2}\pi \ , \quad k=0,1,\ldots,2M-1 \ . \tag{15a}$$

$$I_k \ \text{ root of } \ \left|\alpha J_M'(r) J_L\left(\frac{\varepsilon M}{\Omega}\right)\right| = \frac{\Delta}{M} \ . \tag{15b}$$

with $r = (2I_1)^{1/2}$, $(\,'\,) \equiv \frac{1}{r}\frac{\partial}{\partial r}$. According to (15b) when Δ is small, but not exactly zero, the threshold for the appearance of the chain of first order islands is given by

$$\alpha > \left|\frac{1}{J_M'(r_{max})} \ \frac{\Delta}{J_L\left(\frac{\varepsilon M}{\Omega}\right)}\right| \equiv \alpha_1 \ , \tag{16}$$

and r_{max} is the value that maximizes $|J_M'(r)|$. Since Δ is of order Ω, α_1 is lower than the limit for primary island chain appearance in the uniform-$\underset{\sim}{B}$ case by a factor $\Delta/J_L(\varepsilon M/\Omega)$ which, depending on the parameters, can be much less than 1.

One can now try an evaluation of the new stochasticity threshold due to the interaction between the two close to resonance terms (M,L) and (M,L+1) in the spirit of the approximation Eq. (10). Assuming that the condition

$$|\Delta(M,L)| < \alpha' < |\Delta(M,L+1)|$$

holds, only the (M,L) chain of islands appears initially. It is observed numerically that chaotic behavior sets in as a result of the blow up of the stochastic layer around the primary islands. An analytic method developed lately[14,15] for the evaluation of the

stochasticity threshold in systems demonstrating one primary resonance is used here. The method is described in Appendix B. The result for the new stochasticity threshold is

$$\alpha_s' = \frac{\pi}{18} \frac{\Omega}{M|J_L(\frac{\varepsilon M}{\Omega})|\,|J_M(r_K)J_M''(r_K)|^{1/2}} . \tag{17}$$

The accepted value for the stochasticity threshold in the uniform $\underset{\sim}{B}$-field case $A_s = \frac{1}{4}$ can also be written as

$$\alpha_s \cong \frac{1}{4M}|J_M(r_K)J_M''(r_K)|^{-1/2} .$$

Consequently the ratio of the new threshold to the old one is approximately equal to

$$\alpha_s'/\alpha_s \cong \frac{\Omega}{|J_L(\frac{\varepsilon M}{\Omega})|} \cdot \frac{4\pi}{18} . \tag{18}$$

In case that $\frac{\varepsilon M}{\Omega} \cong x_n$ with x_n a zero of $J_L(x)$, $J_{L+1}(\frac{\varepsilon M}{\Omega})$ must be substituted in the denominator of Eq. (17), in place of $J_L(\frac{\varepsilon M}{\Omega})$, according to the paragraph after Eq. (13). The ratio α_s'/α_s can be much less than 1 if the denominator $J_L(\varepsilon M/\Omega)$ is not very small, i.e.,

$$L \lesssim \varepsilon M/\Omega \quad \text{or} \quad |\nu - M| \equiv |\delta_0| < \varepsilon M \simeq \varepsilon\nu . \tag{19}$$

Recalling the notation used in Sec. I, namely

$$\delta_j = \delta_0 + \varepsilon\nu \sin 2\pi j\Omega \ ,$$

the condition $\varepsilon\nu > |\delta_0|$ simply means that δ_j, the modulated frequency mismatch, can go through zero. A big reduction in stochasticity threshold and diffusion occurs due to $\delta_j = 0$ resonance, thus reaffirming one of the conclusions in Ref. 4.

Figures (5a)-(5d) illustrate the transition to chaotic behavior for $\nu = 20.10$, $\Omega = 0.01$ as the wave amplitude is gradually increasing from $\alpha = 0.0995$ to $\alpha = 0.199$ to $\alpha = 0.398$ and $\alpha = 1.194$ respectively. Ten particles have been followed for $t = 2251$ gyroperiods, starting with initial perpendicular velocities $45. < r < 55.$. In Fig. (5d) the motion is chaotic while α is still less than 1/4 of the uniform field stochasticity threshold.

One should not conclude that in the limit $\Omega \to 0$, $\alpha_s' \to 0$ following Eq. (18). When Ω is extremely small, successive resonant values of ν become so dense that the resonant Hamiltonian Eq. (10) must include many more terms than one. Then relation (18) does not hold. Now, Ω tends to zero when either $P_z \to 0$, or when k ripple $\to 0$ meaning that the scale length of the magnetic field tends to infinity. In either case, it will take infinite time for the particle to feel the effect of the inhomogeneity, and the finite-time behavior will be determined by the uniform field approximation.

Now, assuming that the wave amplitude is well above the stochasticity threshold, an estimate can be given for the extent of the stochastic regime ΔI_s in phase space. When the last KAM surface is destroyed, the stochastic layers around each island are interconnected; thus, the extent of the stochastic regime is roughly equal with the

distance between the innermost and outermost islands in phase space. The centers of these islands are given approximately (from Eq. (15b)) by

$$r_1 \cong \nu \ , \ r_2 \cong \left(\frac{\alpha\pi\,|J_L(\frac{\varepsilon M}{\Omega})|}{\Delta\nu^{1/2}}\right)^{2/3}\nu$$

where the large argument approximation for the Bessel function is used for $r_2 >> \nu$. Consequently,

$$\Delta I_s \cong \frac{1}{2}\,(r_2^2 - r_1^2) \sim O(\nu^2) \ .$$

Thus the modulation has a rather global effect spreading stochasticity over an extended regime. On the other hand, the effect of a slow modulation acting on a non-degenerate Hamiltonian studied by Chirikov[16] (1979) and Tennyson[17] (1979), is localized, creating a rather narrow stochastic band of width $\delta I_s = 2\varepsilon\Omega$.

IVB. Second Order Islands

So far the analysis has been based on the effect of first order resonant terms. They dominate the behavior of the system provided that their amplitudes are not negligibly small, guaranteed by the condition (19). In the opposite case, when $L = \mathrm{Int}(\frac{v-M}{\Omega}) > \varepsilon M/\Omega$, the resonant term coefficients $J_\ell(\varepsilon M/\Omega)$ with ℓ's close to L are negligibly small, and the first order islands do not appear for small values of α and $\Delta \neq 0$. (Even for Δ exactly zero, the contribution of the nonresonant terms becomes dominant and drives the particle out of the first order

resonance.) Then, resonant terms quadratic in α can become the dominant driving force in Hamiltonian (9). These terms, which are not explicitly represented in Eqs. (9a) and (9b), are generated by nonlinear interaction, (i.e., "beating together") between any two terms linear in α and emerge from the Hamiltonian through the canonical transformation $(\tilde{I}_1, \tilde{I}_2, \tilde{\vartheta}_1, \tilde{\vartheta}_2) \to (V_1, V_2, \varphi_1, \varphi_2)$ derived from the generating function

$$F(\tilde{I}_1,\tilde{I}_2,\varphi_1,\varphi_2) \equiv -\tilde{I}_1\varphi_1-\tilde{I}_2\varphi_2 - \alpha \sum_{m,\ell} J_m((2\tilde{I}_1)^{1/2})J_\ell(\frac{\varepsilon m}{\Omega}) \frac{\cos[m\varphi_1-(\nu-\ell\Omega)\varphi_2]}{m-(\nu-\ell\Omega)}$$

namely,

$$\begin{aligned}
\tilde{\vartheta}_1 &= \varphi_1 + \alpha\sum_{m,\ell} J_m'(\tilde{I}_1)\ J_\ell\ (\frac{\varepsilon m}{\Omega}) \frac{\cos[m\varphi_1-(\nu-\ell\Omega)\varphi_2 + \frac{\ell\pi}{2}]}{m-(\nu-\ell\Omega)} , \\
\tilde{\vartheta}_2 &= \varphi_2 , \qquad\qquad (20) \\
V_1 &= \tilde{I}_1 - \alpha \sum_{m,\ell} \frac{mJ_m(\tilde{I}_1)J_\ell(\frac{\varepsilon m}{\Omega})}{m-(\nu-\ell\Omega)} \sin[m\varphi_1-(\nu-\ell\Omega)\varphi_2 + \frac{\ell\pi}{2}] , \\
V_2 &= \tilde{I}_1 + \alpha \sum_{m,\ell} \frac{(\nu-\ell\Omega)J_m(\tilde{I}_1)J_\ell(\frac{\varepsilon m}{\Omega})}{m-(\nu-\ell\Omega)} \sin[m\varphi_1 - (\nu-\ell\Omega)\varphi_2 + \frac{\ell\pi}{2}] .
\end{aligned}$$

The sums involved in Eq. (20) converge and the transformation is close to an identity if

$$\alpha < |\Delta(M,L)|$$

Then $K' \to \Lambda$, where

$$\Lambda \cong V_1+V_2 - \frac{\alpha^2}{2} \sum_{n,k} \frac{J_n'((2V_1)^{1/2})J_k(\frac{\varepsilon n}{\Omega})}{n-(\nu-k\Omega)} \sum_{m,\ell} J_m((2V_1)^{1/2})J_\ell(\frac{\varepsilon m}{\Omega})$$

$$\times \left\{\cos\left[(m+n)\varphi_1-(2\nu-(\ell+k)\Omega)\varphi_2 + \frac{\ell+k}{2}\pi\right] + \cos\left[(m-n)\varphi_1+(\ell-k)\Omega\varphi_2 + \frac{\ell-k}{2}\pi\right]\right\} . \quad (21)$$

The above transformation is equivalent to phase averaging out all terms linear in α when first-order resonances do not appear. Instead, 2nd order resonant terms emerge for all these combinations of the four independent integer parameters m,n,ℓ,k which satisfy

$$|(m+n) - (\ell+k)\Omega-2\nu| < \frac{1}{2}\Omega .$$

Let $M_0 = \mathrm{Int}(2\nu)$, $L_0 = \mathrm{Int}\left((2\nu-M_0)/\Omega\right)$. Using the same kind of arguments as in the previous subsection to select the dominant terms in the expansion,[18] the approximation for the resonant Hamiltonian is

$$\Lambda_R' \cong V_1' + (2\nu-L_0\Omega)V_2' - \frac{\alpha^2}{2} C(r)J_{L_0}\left(\frac{\varepsilon M_0}{\Omega}\right) \sin\left[M_0\varphi_1' - \varphi_2' + \frac{(L_0-1)\pi}{2}\right] \quad (22)$$

with

$$V_1' = V_1 , \qquad \varphi_1 = \varphi_1' ,$$

$$(2\nu-L_0\Omega)V_2' = V_2 , \qquad (2\nu-L_0\Omega)\varphi_2 = \varphi_2' ,$$

$$r = (2V_1')^{1/2}$$

and

$$C(r) = \left\{\frac{J'_{M_0}(r)J_0(r)}{M_0-(\nu-L_0\Omega)} - \frac{J'_0(r)J_{M_0}(r)}{\nu}\right\} .$$

Figure 6 is a surface of section for $\nu = 15.575$ showing the presence of 2nd order islands. Note that the number of stability islands is $M_0 = 31 = \mathrm{Int}(2\nu)$ showing that the resonant part of the Hamiltonian, Λ_R, dominates the evolution of the system. The structure of Λ'_R is the same as K'_R. Then we can easily estimate a new stochasticity threshold due to the blow up of the stochastic regime by repeating the same procedure as for the first order islands. It is found that

$$\alpha''_s/\alpha_s \cong \frac{M|J_M(r_1)|^{1/2}}{M_o^{1/2}|C(r_2)C''(r_2)|^{1/4}} \left\{\frac{2\Omega}{|J_{L_0}(\frac{\varepsilon M_0}{\Omega})|}\right\}^{1/2} , \tag{23}$$

where r_1, r_2, respectively satisfy $J'_M(r_1) = 0$, $C'(r_2) = 0$, and α''_s is the new stochasticity threshold due to secondary island overlapping.

Observe that α''_s/α is roughly equal to $(\alpha'_s/\alpha_s)^{1/2}$, with α'_s given by Eq. (18). Again a''_s/α_s can be much lower than 1 if $J_{L_0}(\varepsilon M_0/\Omega)$ is not too small, i.e., $L_0 \lesssim \frac{\varepsilon M_0}{\Omega}$. Then, $L_0\Omega \cong |2\nu-M_0| < \varepsilon M_0 \cong 2\varepsilon\nu$, or $|\nu - M_0/2| < \varepsilon\nu$. When $M_0 = 2M+1$, the above means $|\nu-M-1/2| < \varepsilon\nu$ or

$$|\delta_0 - \frac{1}{2}| < \varepsilon\nu . \tag{24}$$

Recalling the notation in Sec. I

$$\delta_j = \delta_0 + \varepsilon\nu \sin 2\pi j\Omega \ ,$$

condition (24) means that, even if the system does not go through the $\delta_j = 0$ resonance, a big reduction in stochasticity threshold and diffusion occur if it can go through the $\delta_j = 1/2$ resonance.

A final word must be said for higher order resonances, $O(\alpha^3)$. When α is less than a threshold α_2 given by

$$\alpha < \alpha_2 \equiv \left| \frac{2\Delta'}{M_0 J_{M_0}((2J_1)^{1/2}) J_{L_0}(\frac{\varepsilon M_0}{\Omega})} \right|^{1/2}$$

with $|\Delta'| \equiv |2\nu - M_0 - L_0\Omega|$, second order stationary points disappear. Then one must look for resonances of higher order. Assume that ν is such that a resonance appears for an integer p satisfying

$$\Delta'' \equiv p\nu - (m_1+m_2+m_3) - (\ell_1+\ell_2+\ell_3)\Omega \cong 0 \ .$$

Following the same line of thought as earlier in this section, one expects that the island chain corresponding to the above resonance will dominate the evolution of the system if

$$L_p < \frac{\varepsilon M_p}{\Omega} \ , \ M_p = \mathrm{Int}(p\nu), \ L_p = \mathrm{Int}\left(\frac{p\nu - M_p}{\Omega}\right) \ . \tag{25}$$

This is equivalent to $|\delta_j - \frac{1}{p}| < \varepsilon\nu$ or δ_j going through the 1/p resonance of the uniform $\underset{\sim}{B}$-field case. The stochasticity threshold induced by these higher order islands overlapping is expected to be higher than α_s', α''_s but it may still be lower than α_s. However, it has

been established[4] that the resulting diffusion is much slower and of no practical importance for LH heating.

The connection between the results obtained here using Hamilton's equations, and these obtained in Ref. 4 using Eqs. (1) and (2) as a simple model should be clear now. The passage of δ_j through the $\delta=0$ resonance of the uniform B-field case coincides with the emergence of finite amplitude first order resonant terms in the new Hamiltonian for the non-uniform $\underset{\sim}{B}$-field. When δ_j can not go through 0, the parameters are such that the amplitudes of the first order resonant terms in Hamiltonian (9b) become negligibly small. However, the second order resonant terms in Eq. (21) will grow to significant amplitudes if δ_j can go through 1/2. Resonances of even higher order are dominant if δ_j can go through a q/p resonance, q,p integers. When $\varepsilon\nu \sim 1$, all kinds of resonant terms are important since δ_j sweeps all values between 0 and 1. Then the thresholds α_s', α_s'' derived for small ε and the one resonance approximation can only serve as upper bounds for the new threshold.

V. DERIVATION OF THE NONAUTONOMOUS MAP

The nonautonomous map Eqs. (1) and (2) used in earlier work to model the system and study the diffusion induced by the inhomogeneity of the magnetic field will be derived here from the two-dimensional autonomous Hamiltonian (7) derived in Section II.

The reader may be alerted at this point by an apparent contradiction stemming from the fact that a two-dimensional nonautonomous map is derived from a two-dimensional autonomous

Hamiltonian system. It will become clear, though, that the explicit time dependence of the map is not generic but a result of an approximation. A two-dimensional autonomous map will be derived initially, yielding the nonautonomous term by keeping only linear terms in the small parameters.

The method of the derivation is similar to the one applied for the derivation of the uniform $\underset{\sim}{B}$-field map.[2] The procedure is reviewed in detail in Appendix C. As a result, the auxiliary variables

$$u = \vartheta-\rho \quad , \quad v = \vartheta+\rho$$

are introduced where

$$\rho \cong (2I_1')^{1/2} + (n+1/4)\pi$$

$$\vartheta = n\vartheta_1-\vartheta_2 \ . \tag{26}$$

These variables obey the following equations of motion

$$\dot{u} = \delta(t) - 2\pi A\cos\left[v-(\pi-\xi)\delta_0\right] \sum_{j=-\infty}^{\infty} \hat{\delta}(t-\xi-2\pi j) \ ,$$

$$\dot{v} = \delta(t) + 2\pi A\cos\left[u+(\pi-\xi)\delta_0\right] \sum_{j=-\infty}^{\infty} \hat{\delta}(t-\xi-2\pi j) \ , \tag{27}$$

with

$$\delta(t) \equiv \delta_0 + \varepsilon n\sin\Omega t \cong \delta_0 + \varepsilon\nu\sin\Omega t \ .$$

Let t_j be the time a particle crosses for the jth time the $q_y = 0$ plane with velocity $Q_y < 0$, i.e., the reduced gyroangle $\vartheta_1 = (2j+1)\pi$ plane. Then from Eqs. (26)

$$\vartheta(j) = n\pi - n\vartheta_1(j) + \vartheta_2(j) = \vartheta_2(j) - 2\pi n(j+1) \ ,$$

thus $\vartheta(j) \equiv \vartheta_j$ coincides with the phase ϑ_2 of the wave at the surface of section. From Eq. (7), $t_j = \vartheta_j/\nu = (v_j+u_j)/2\nu$, i.e., the time t_j at the surface of section can be expressed implicitly. Integration of Eqs. (27) over the time interval $t_{j+1} - t_j$ yields

$$\begin{aligned} u_{j+1} - u_j &= \int_{t_j}^{t_{j+1}} dt\ \delta(t) - 2\pi A\cos v_j \ , \\ v_{j+1} - v_j &= \int_{t_j}^{t_{j+1}} dt\ \delta(t) - 2\pi A\cos u_{j+1} \ . \end{aligned} \tag{28}$$

The integral in the right-hand side of Eqs. (28) can be approximated by a linear expansion as

$$\begin{aligned} \int_{t_j}^{t_{j+1}} dt\ \delta(t) &= \delta_0(t_{j+1}-t_j) + \varepsilon\nu\sin(\Omega t_j)(t_{j+1}-t_j) \\ &\quad + \frac{\Omega}{2}\ \varepsilon\nu\cos(\Omega t_j)(t_{j+1}-t_j)^2 + \ldots \ . \end{aligned}$$

Using

$$t_{j+1} - t_j = \frac{\vartheta_{j+1} - \vartheta_j}{\nu}$$

we obtain

$$u_{j+1} - u_j = 2\pi[\delta_0 - \varepsilon\nu\sin\frac{u_j+v_j}{2\nu}\Omega] - 2\pi A\cos v_j + O(2\pi^2\varepsilon\nu\Omega A) ,$$

$$v_{j+1} - v_j = 2\pi[\delta_0 - \varepsilon\nu\sin\frac{u_j+v_j}{2\nu}\Omega] + 2\pi A\cos u_{j+1} + O(2\pi^2\varepsilon\nu\Omega A) . \tag{29}$$

The last term on the right is negligible if

$$2\pi^2\varepsilon\nu\Omega << 1 . \tag{30}$$

This is an extra validity condition for the nonuniform $\underset{\sim}{B}$-field map, in addition to the validity conditions for the uniform B-field map

$$r-\nu > (\nu/2)^{1/3} , \qquad \nu >> 1 ,$$

and (31)

$$A << (r^2-\nu^2)^{3/2}/r^2 ,$$

(the last one meaning that the change in A during a cycloperiod, $1/A\ dA/d\rho$, is very small). Equation (30) guarantees that the modulation frequency Ω is so slow that $\delta(t)$ can be considered constant during one cycloperiod.

Observe that Eq. (29) is a two-dimensional autonomous map which is naturally expected from a two-dimensional Hamiltonian. A further approximation

$$\vartheta_j = 2\pi\nu j + O(A)$$

and a linear expansion of the sine term into the brackets in Eq. (29) leads, after dropping terms of order $\varepsilon\Omega A$, to

$$u_{j+1}-u_j = 2\pi\delta_j - 2\pi A\cos v_j \ ,$$

$$v_{j+1}-v_j = 2\pi\delta_j + 2\pi A\cos u_{j+1} \ , \tag{32}$$

where

$$\delta_j = \delta_0 + \varepsilon\nu\sin 2\pi j\Omega \ .$$

The above form is identical to the nonautonomous approximation Eqs. (1),(2). Comparison between the diffusion coefficients calculated by numerically iterating (29) and (32) subject to the same initial conditions showed a good agreement, for values of A above the new stochasticity threshold

$$A_s' = \alpha_s' \left(\frac{\pi}{2}\right)^{1/2} \frac{\nu(r^2-\nu^2)^{1/4}}{r^2} = A_s\left[J_L\left(\frac{\varepsilon M}{\Omega}\right)\right]^{-1} \Omega \ . \tag{33}$$

It must not escape our attention though that, for A smaller than A_s', there is a fundamental difference; expression (29) admits A_s' as a threshold below which no diffusion occurs and the derived diffusion coefficient is zero, while map (32), due to higher dimensionality exhibits a very slow diffusive behavior below A_s', similar in spirit to the so-called Arnold diffusion.[5]

VI. MODULATION OF DRIVING FREQUENCY ν

The modulation of the frequency mismatch δ due to the variation of the particle gyroperiod was shown to be the main mechanism for low amplitude, wave induced diffusion. It is obvious that δ can also be modulated by externally varying the frequency of the driving electrostatic wave. Here, it will be proven that exactly the same situation arises in the case of a particle in a <u>uniform</u> magnetic field under the influence of an externally imposed wave with <u>modulated frequency</u>. Consequently, it can be argued that, in a system of two coupled oscillators subject to frequency modulation, it is the variation in the mismatch between the oscillator's fundamental frequencies that determines the diffusive behavior of the system.

Consider the Hamiltonian Eq. (7) with $\varepsilon=0$ (i.e., uniform $\underset{\sim}{B}$-field) and introduce a variation in the driving wave frequency,

$$\nu \rightarrow \nu(t) = \nu(1-\varepsilon'\cos \Omega t) \ .$$

The phase of the wave will be given by

$$\varphi(t) = \nu t - \varepsilon'\nu/\Omega \sin \Omega t$$

and the Hamiltonian $\tilde{K}(\tilde{I}_1, \tilde{\vartheta}_1, \tilde{I}_2, \tilde{\vartheta}_2)$ by

$$\tilde{K} = \tilde{I}_1 + \tilde{I}_2 - \alpha \sin\{(2\tilde{I}_1)^{1/2}\sin\tilde{\vartheta}_1 - \nu[\tilde{\vartheta}_2 - \frac{\varepsilon'}{\Omega} \sin\Omega\tilde{\vartheta}_2]\} \ , \qquad (34)$$

with $\tilde{I}_1$, $\tilde{I}_2$, $\tilde{\vartheta}_1$, $\tilde{\vartheta}_2$, obtained by setting $\varepsilon=0$ in Eqs. (9a), Sec. II, i.e.,

$$\tilde{I}_2 = vI_2 \ , \qquad \vartheta_2 = \nu\tilde{\vartheta}_2 \ ,$$

$$\tilde{I}_1 = I_1 = \frac{1}{2}\left(P_y^2+y^2\right) \ , \qquad \vartheta_1 = \tilde{\vartheta}_1 = \tan^{-1}\left(\frac{y}{P_y}\right) \ .$$

It is expanded according to

$$\tilde{K} = \tilde{I}_1 + \tilde{I}_2 - \alpha \sum_m \sum_\ell J_m\left[(2\tilde{I}_1)^{1/2}\right] J_\ell\left(\frac{\varepsilon'\nu}{\Omega}\right) \sin\left[m\tilde{\vartheta}_1 - (\nu-\ell\Omega)\tilde{\vartheta}_2\right] \ . \qquad (35)$$

Expression (35) is the same as expression (9), the only difference being that m in the argument of the Bessel functions $J_\ell(\varepsilon m/\Omega)$ in Eq. (9) has been replaced by ν in Eq. (35). Nevertheless, it was already explained that the essential contribution for diffusion comes from the resonant term $M\cong\nu$. Thus, the resonant form of Hamiltonian (35) is identical to that of Eq. (9) and so the analysis and the thresholds derived in Sec. IV are still holding. In order to see that the map (29) is applicable in the case of the wave frequency modulation one can reintroduce a finite ε by setting $\varepsilon' = \varepsilon \dfrac{(2\tilde{I}_1(0))^{1/2}}{\nu} = \varepsilon \dfrac{(2\tilde{I})^{1/2}}{\nu} + O(\lambda^2)$, and treating ε as constant over a small range of $\tilde{I}_1$. Substituting the above in Eq. (34) and then inverting the transformations Eq. (9a),

$$\nu\hat{I}_2 = \tilde{I}_2 + \varepsilon\tilde{I}_1\sin\Omega\tilde{\vartheta}_2 \ , \qquad \hat{\vartheta}_2 = \frac{1}{\nu}\tilde{\vartheta}_2 \ ,$$

$$\hat{I}_1 = \tilde{I}_1 \ , \qquad \tilde{\vartheta}_1 = \hat{\vartheta}_1 - \frac{\varepsilon}{\Omega}\cos\frac{\Omega}{\nu}\hat{\vartheta}_2 \ ,$$

expression (34) takes the form of Hamiltonian (7) with $(\hat{I}_1,\hat{I}_2,\hat{\vartheta}_1,\hat{\vartheta}_2)$ in place of $(I_1,I_2,\vartheta_1,\vartheta_2)$. Then, according to Sec. V, the same autonomous

map (29) derived from Hamiltonian (7) can be used to study the properties of motion irrelevantly to whether the modulation δ_j comes from the toroidal ripple or the external frequency modulation. However, the physical meaning of ρ_j, ϑ_j calculated at the end of the j-th "reduced" gyroperiod $\vartheta_1(j) = (2j+1)\pi$, as well as the reduced gyroangle itself, are slightly different in each case, according to the following

<u>cyclotron frequency modulation</u>	<u>wave frequency modulation</u>
$\omega_c = (1-\varepsilon \sin\Omega t)$	$\nu(t) = \nu(1-\varepsilon' \cos\Omega t)$
ε	$\varepsilon=\varepsilon' \frac{\nu}{r}$
$\rho_j \cong v_{\perp j}(1-\varepsilon \sin\Omega t_j)^{1/2}$	$\rho_j \cong v_{\perp j}$
$\vartheta_j = vt_j$ = phase of the wave	$\vartheta_j = vt_j$ = phase of the wave + $\frac{v\varepsilon'}{\Omega} \cos \Omega t_j$

reduced gyroangle

$\vartheta_1 = \tan^{-1}[(1-\varepsilon \sin\Omega t) \frac{y}{P_y}]$	$\hat{\vartheta}_1 = \tan^{-1} (\frac{y}{P_y}) + \frac{\varepsilon}{\Omega} \cos\Omega t$

To illustrate the potential benefits of frequency modulation during heating, the new stochasticity thresholds are calculated numerically here, using the map (29) and their values are compared with the analytic prediction, Eq. (17). To estimate the new thresholds 10^2 particles are initially distributed inside a regime bounded by adjacent separatrices (trajectories that connect unstable fixed points). The particles are followed for about 40,000 cycloperiods. Parameters ε and ν are kept constant and Ω is changing, allowing a more thorough test of Eq. (17), since not only the argument but also the order L of the Bessel function in the denominator is changing $\left(L = \frac{\nu-M}{\Omega}\right)$. It is always arranged that $\Delta = \nu-M-L\Omega = 0$. In that case the form of separatrices is simple; they are the curves connecting the unstable fixed points of Hamiltonian Eq. (14) and they are given, using the large argument approximation of the Bessel functions, by rectangles with sides $\sqrt{2I_1} = \sqrt{2nI_\psi} = (p+1/2)\pi + \frac{\pi}{4}$; $\psi = q\pi$. In the variables of the map (29) the separatrices are formed by the intersecting set of lines

$$\frac{v-u}{2} = \rho = (p+1/2)\pi$$

$$\frac{v+u}{2} = \vartheta = q\pi - (2n+1)\pi \ ,$$

p,q,n integers. Here, the particles are initially distributed inside the band $-\frac{\pi}{2} < \rho < \frac{\pi}{2}$. For each set of parameters ε,Ω and ν the value A_s' is taken as the minimum tested value of A before diffusion of particles out of the band ceases. The minimum initial distance from the ρ-boundaries is such that crossing of the separatrices corresponds to a growth of the stochastic layer around the separatrices to a half

width $h \cong \pi/20$. In Fig. (7) the numerical results $A_s'/A_s = \alpha'_s/\alpha_s$ are plotted against the theoretical predictions of Eq. (17). Good agreement is shown. Lower thresholds occur for small Ω, however the diffusion rate[4] is higher with modest Ω. In conclusion, externally varying the frequency of the launched LH waves appears to be a promising method to lower the wave amplitude threshold for effective ion energy absorption, with the additional advantage of making it possible to control the modulation parameters ε and Ω. Since typical values of Ω and ε of order $\sim 10^{-2}$ will be sufficient, the change in the position of the resonant layer δR_{res} due to the change of $\nu = \omega_{LH}/\omega_c$, according to

$$\frac{\delta R_{res}}{R} = \left(\frac{d}{dr}\left[\omega_{LH}/\omega_c\right]\right)^{-1} \frac{\delta\nu}{R} ,$$

$$\delta\nu \simeq \varepsilon\nu ,$$

will also be small.

VII. LARGE SIZE RIPPLE IN THE MAGNETIC FIELD

Here, the particle motion in an electrostatic wave is examined in the case when there is a large size ripple in the externally applied magnetic field. The above situation can arise during LH heating in compact tori, such as spheromaks, or in the new generation of tokamaks with moderate aspect ratios, such as TFTR, JET or INTOR. When ε is a modest fraction of 1, the small parameter expansion performed in Sec. II that reduced the Hamiltonian in a two-dimensional form, is not

valid. More analytically, the variation in P_z becomes significant and the modulation frequency $\Omega = kP_z$ changes considerably with time. The full set of the equations of motion in three dimensions must be retained. The vector potential $\underset{\sim}{A}$ and the Hamiltonian Eq. (3a), introduced in Sec. II for ε small, can still provide a reasonable approximation under the following simplifying assumptions:

(i) Toroidal effects, such as the grad-B and the curvature drifts, are neglected and particles remain confined on a given flux surface for a long time compared to the time to go around the torus.

(ii) The resonant layer is localized around a flux surface, and the wave amplitude is constant there.

(iii) $\underset{\sim}{B}$ is a periodic function of the length z along a magnetic line on a given flux surface, and has a dominant Fourier component.

The equations of motion, derived from Hamiltonian (3a) are

$$\begin{aligned}
\dot{y} &= P_y \\
\dot{z}_z &= P_z \\
\dot{P}_y &= -y(1 - \varepsilon\sin\kappa z)^2 + \alpha\cos(y-\nu t) \\
\dot{P}_z &= \varepsilon\kappa\cos\kappa z(1-\varepsilon\sin\kappa z)y^2 \ .
\end{aligned} \tag{36}$$

This system of four coupled first order nonautonomous differential equations is solved numerically. Here I will confine myself to reviewing some numerical results. The trajectory of the system is confined on a 5-dimensional surface of the six-dimensional phase space $(I_1, I_2, P_z, \vartheta_1, \vartheta_2, z)$, obtained from (P_x, P_y, P_z, x, y, z) through the transformations Eqs. (3b), (3c). We can consider the 4-dimensional surface of section of the above surface with the plane $\vartheta_2 = 2\pi$ and then

take the projections of the above surface of section $(I_1, P_z, \vartheta_1, z)$ into the (Q_y, q_y), (I_1, ϑ_1) and (P_z, z) planes respectively. $\big((Q_y, q_y)$ and (I_1, ϑ_1) are not independent pairs of variables but simply a coordinate transformation on the same plane.$\big)$ This is achieved by integrating Eqs. (36) numerically for ten ions starting with initial conditions (in normalized units) $15 \leqslant v_\perp \leqslant 30$, and $v_\parallel = 20$, the other parameters being $\alpha = 3.832$ $\nu = 30.243$. Figures (8a) and (8b) represent the uniform field results (ε=0) while the non-uniform field results are plotted in Figs. (9a)-(9c) for $\varepsilon = 0.3$. The major observed change in behavior due to the ripple in the $\underset{\sim}{B}$-field is that heating of ions with initial perpendicular velocity $v_\perp(0) < v_{res} \simeq \omega_{LH}/k_\perp$, $(r(0) < \nu)$ occurs. In other words, the lower limit of the stochastic regime in the $v_\perp$ space is pushed below the resonant velocity v_{res}, resulting in heating of slower ions. For the case under consideration, taking into account the finite wave amplitude correction to include ions trapped in the electrostatic potential, the uniform $\underset{\sim}{B}$-field velocity threshold, is given by

$$r_{min} \simeq \nu - 2\,\alpha^{1/2} \simeq 27 \ ,$$

as seen in Fig. (8b). For the non-uniform field case, we observe from Fig. (9b) that

$$r'_{min} \simeq 19 \simeq 2/3\ r_{min}$$

corresponding to ions with about half the perpendicular thermal energy of the resonant ions. [Note also that the perpendicular energy of some

ions increases above the point $\frac{v_\perp}{v_\parallel} > \varepsilon^{-1/2} \simeq 2$, thus they become trapped in the magnetic ripple, Fig. (9c).]

A rough explanation for the new lower threshold can be attempted as follows. Assume an ion that has an initial speed $v_\perp(0)$ at the bottom of the magnetic ripple $\kappa z = \pi/2$. For short time periods, the zeroth order trajectory conserves the adiabatic invariant μ (expressed in normalized units as I_1), and the total energy is also approximately conserved. Then $v_\perp$ varies roughly as

$$v_\perp(z) = v_\perp(0) \left(\frac{1 - \varepsilon \sin\kappa z}{1-\varepsilon}\right)^{1/2} . \tag{37}$$

Energy absorption from the wave occurs at these points of the cyclotron orbit where the ion resonates with the wave.[1] If the wave amplitude is above the stochasticity threshold then the kicks in $v_\perp$ become uncorrelated and energy diffusion occurs. The resonant condition in the non-uniform $\underset{\sim}{B}$-field case involves both the gyroangle ϑ_1 and the z-position,

$$v_\perp(z)\sin\vartheta_1 = \frac{\omega_{LH}}{k_\perp} - 2\left(\frac{|e|E_0}{k_\perp m}\right)^{1/2}$$

and is written in normalized units as

$$r(z)\sin\vartheta_1 = \nu - 2\,\alpha^{1/2} . \tag{38}$$

It is easily seen that the minimum value $r'_{min} = r(0)$ the ion must have,

so that r(z) resonates with the wave at some z, is given combining (37) and (38) by

$$r'_{min} = (\nu - 2\ \alpha^{1/2})\ \left(\frac{1-\varepsilon}{1+\varepsilon}\right)^{1/2} \approx (1-\varepsilon) r_{min}\ . \tag{39}$$

If $E_m = \frac{1}{2}\, m v_{min}^2$ is the energy of the slowest ion accelerated in the uniform field situation, the corresponding lowest energy due to the effect of the ripple is

$$E'_m = \frac{1}{2}\, m v'^2_{min} \cong (1-2\varepsilon) E_m\ .$$

Assuming a maxwellian distribution, the number of heated particles increases by a factor of

$$q \cong f(E'_m)/f(E_m) \cong e^{2\varepsilon E_m/kT}\ . \tag{40}$$

Typically the ratio $E_m/kT = \frac{v_{res}^2}{v_{th}^2} >> 1$, thus the resulting increase is quite significant. For example, in the Alcator A heating experiment,[19] $v_{res}/v_{th} \cong 5.2$, $\varepsilon = .06$ yielding $q \cong 2.5\times10^1$. In Fig. 10 numerical results for $r'_{min} \equiv v_\perp$ as a function of the ripple size ε are plotted against the theoretical prediction of Eq. (39) (solid line) for a fixed wave amplitude well above the stochasticity threshold. Good agreement is observed.

VIII. CONCLUSION

The presence of a ripple in the magnetic field due to toroidal effects was found to enhance RF power absorption by lowering the wave amplitude thresholds and enlarging the stochastic regime in the velocity space. Results obtained during a series of Alcator A lower hybrid heating experiments have been analyzed in Ref. 19. It was pointed out there that the launched wave amplitude remained well below the uniform B-field stochasticity threshold, due to the distribution of the wave energy over a wide regime in the torus. However, the observed heating can be accounted for if the reduction in the threshold due to the magnetic field ripple is taken into account.[4] A frequency modulation of the launched waves will have equivalent effects and is proposed as a method of improving energy absorption. Some other effects such as non-monochromatic wave spectra, incoherency, propagation effects[20,21] and scattering[22,23] need to be considered for a full picture of the lower hybrid heating situation. From the theoretical standpoint the effect of a slow modulation on an intrinsically degenerate Hamiltonian was considered and found to have more pronounced effects than in the case of the "modulational instability" in non-degenerate Hamiltonians.

ACKNOWLEDGMENTS

I would like to thank H. Varvoglis for many fruitful discussions. Useful discussions with D. F. Escande and E. Ott are also gratefully acknowledged.

Work on this paper was supported by the U. S. Department of Energy grant no. DE-FG05-80ET-53088.

Appendix A

(a) Derivation of Hamiltonian Eq. (4) from Eq. (3a)

Let

$$q_y = (1-\varepsilon\sin\kappa z)^{1/2} y \ , \qquad Q_y = (1-\varepsilon\sin\kappa z)^{-1/2} P_y \ ,$$

$$q_z = z \ , \qquad Q_z = P_z - \frac{\varepsilon\kappa\cos\kappa z}{1-\varepsilon\sin\kappa z} P_y y \ , \tag{A1}$$

a canonical transformation introduced by the generating function

$$S(Q_y, Q_z, y, z) \equiv (1-\varepsilon\sin\kappa z)^{1/2} Q_y y + Q_z z \ .$$

The transformed Hamiltonian becomes

$$H = \frac{1}{2}(1-\varepsilon\sin\kappa q_z)(q_y^2+Q_y^2) + \frac{1}{2}\left(Q_z + \frac{\varepsilon\kappa\cos\kappa q_z}{1-\varepsilon\sin\kappa q_z} Q_y q_y\right)^2$$

$$- \alpha \sin[q_y/(1-\varepsilon\sin\kappa q_z)^{1/2} - \nu t] \ . \tag{A2}$$

Under a new canonical transformation given by the generating function

$$S_1 = \frac{1}{2} y^2 \cot\vartheta_1 \ ,$$

so that

$$q_y = (2I_1)^{1/2} \sin\vartheta_1 \ ,$$

$$Q_y = (2I_1)^{1/2} \cos\vartheta_1 \ , \tag{A3}$$

the new Hamiltonian is

$$H_1 = (1-\varepsilon\sin\kappa q_z)I_1 + \frac{1}{2}\left(Q_z + \frac{\varepsilon\kappa\cos\kappa q_z}{1-\varepsilon\sin\kappa q_z} I_1\sin 2\vartheta_1\right)^2$$

$$- \alpha\sin\{[2I_1/(1-\varepsilon\sin\kappa q_z)]^{1/2}\sin\vartheta_1 - \nu t\} \ . \tag{A4}$$

An approximate Hamiltonian $K \cong H_1$, linear in the small parameters will be introduced. Letting

$$\alpha, \ \varepsilon, \ \kappa \sim O(\lambda) \quad , \quad \lambda << 1$$

and noticing from Eq. (3b) that

$$Q_z = P_z + O(\lambda^2) \cong P_z \ , \quad z = q_z \ ,$$

we obtain Eq. (4)

$$K(\vartheta_1, z, I_1, P_z; t) \equiv (1-\varepsilon\sin\kappa z)I_1 + \frac{1}{2}P_z^2 - \alpha\sin[(2I_1)^{1/2}\sin\vartheta_1 - \nu t] \ . \tag{A5}$$

(b) Derivation of Hamiltonian Eq. (6)

By inspection of Eqs. (5a) and (5b) one sees that resonant terms in the (I_1,ϑ_1) plane motion come through the term $\alpha\ \partial K_1/\partial\vartheta_1 \sim O(\lambda)$, while resonant behavior in (P_z,z) plane comes through terms of order $\varepsilon\kappa \sim O(\lambda^2)$, or higher. Consequently a perturbative solution of Eq. (5b) for $P_z(t)$ and $z(t)$ is satisfactory to order λ. One then substitutes into Eq. (5b) to obtain a pair of nonautonomous differential equations for I_1, ϑ_1. From (5b),

$$P_z(t) = P_z(0) - \varepsilon\,\frac{I_1(0)}{P_z(0)}\sin\Omega t\ ,$$

$$z(t) = P_z(0)t + \varepsilon[\cos\Omega t-1]\,\frac{I_1(0)}{\Omega P_z^2(0)} + z(0)\ , \tag{A6}$$

$$\Omega = \kappa P_z(0)\ .$$

Having expressed z, P_z as explicit functions of time and initial conditions only, Eq. (5a) describing the motion in the (I_1,ϑ_1) plane can be derived from the one-dimensional, nonautonomous Hamiltonian

$$K(I_1,\vartheta_1;t) = \{1 - \varepsilon\ \sin[\Omega t + \varepsilon\,\frac{I(0)}{P_z^2(0)}\,(\cos\Omega t-1)]\}I_1$$

$$- \alpha\ \sin\{(2I_1/(1-\varepsilon\ \sin\Omega t))^{1/2}\sin\vartheta_1-\nu t\}\ ,$$

Dropping the terms of order λ^2, we obtain Eq. (6)

$$K \cong (1-\varepsilon\sin\Omega t)I_1 - \alpha\ \sin[(2I_1)^{1/2}\sin\vartheta_1-\nu t]\ . \tag{A7}$$

Appendix B

The stochasticity threshold, Eq. (17), is evaluated following Ref. 15. Hamiltonian Eq. (10) is expressed in the $(I_\psi, I_\varphi, \psi, \varphi)$ variables as

$$\underset{\sim}{K} = -\Delta I_\psi + \frac{\Delta}{M} I_\varphi$$

$$-\alpha J_M(r) J_L\left(\frac{\varepsilon M}{\Omega}\right)\sin\left(\psi + \frac{L\pi}{2}\right) \quad . \tag{B1}$$

$$-\alpha J_M(r) J_{L+1}\left(\frac{\varepsilon M}{\Omega}\right)\sin\left(\psi - \frac{M\Omega}{\Delta}\varphi + \frac{(L+1)\pi}{2}\right)$$

Expanding around the fixed points of $\underset{\sim}{K}_R$, Eqs. (15a,b) in the new canonical variables $\underset{\sim}{\psi} = \psi - \psi_K$, $\underset{\sim}{I}_\psi = I_\psi - I_K$ and solving for $\varphi = \frac{\Delta}{M} t$ one obtains

$$h = \frac{1}{2}\alpha_L M^2 J_M''(r_K)\underset{\sim}{I}_\psi^2 - \alpha_L J_M(r_K)\cos\underset{\sim}{\psi} - \alpha_{LH} J_M(r_K)\cos\left(\underset{\sim}{\psi} - \Omega t + \frac{\pi}{2}\right)$$

renormalized to

$$\tilde{h} = \frac{1}{2}\underset{\sim}{I}_\psi^2 - Q\cos\underset{\sim}{\psi} - P\cos\left[g(\underset{\sim}{\psi} - \Omega t) + \frac{\pi}{2}\right] \tag{B2}$$

with

$$\alpha_L = J_L\left(\frac{\varepsilon M}{\Omega}\right)$$

$$Q = \alpha_L^2 M^2 J_M(r_K) J_M''(r_K) \quad , \tag{B3}$$

$$P = \alpha_L \alpha_{L+1} M^2 J_M(r_K) J_M''(r_K) \quad .$$

This is the standard form used in Ref. 15 to obtain the following criterion:

$$\rho_s \geqslant [\lambda+2 - 2(\lambda+1)^{1/2}]/\lambda^2 \tag{B4}$$

with

$$\rho = 2\sqrt{|Q|}/\pi g \quad ,$$

$$s \quad \text{defined by} \quad P/Q \sim O(\rho^s)$$

$$\lambda = 2g+1-s \quad .$$

Here g=1, s=0 yielding λ=3 and by combining (B3) and (B4)

$$\alpha_s' = \frac{\pi}{18} \; \frac{\Omega}{M|J_L(\frac{\varepsilon M}{\Omega})|\,|J_M(r_K)J_M''(r_K)|^{1/2}} \quad . \tag{B5}$$

Appendix C

Hamiltonian (7) can be transformed into

$$M \equiv -[\delta_0+\varepsilon n \sin \frac{\Omega}{\nu} X_2]h_1+\nu h_2-\alpha \sum_k J_{n+k}[(nh_1)^{1/2}]\sin[(1+\frac{k}{n})X_1+\frac{k}{n} X_2] \qquad (C1)$$

through

$$X_1 = n\vartheta_1-\vartheta_2 , \qquad I_1 = nh_1 ,$$
$$X_2 = \vartheta_2 , \qquad I_2 = h_2-h_1 , \qquad (C2)$$

derived from the generating function

$$S(h_1,h_2,\vartheta_1,\vartheta_2) \equiv (n\vartheta_1-\vartheta_2)h_1 + \vartheta_2 h_2 .$$

Here $\delta_0 = \nu-n$, n being the closest integer to $\nu = \omega/\omega_{co}$. The essential contribution comes from $k << n$. Performing a large argument expansion of $J_m(r)$, valid if $r > m + (m/2)^{1/3} \cong (n+k) + (n/2)^{1/3}$, approximating $(r^2-m^2)^{-1/4}$ as $(r^2-\nu^2)^{-1/4}$, valid if $r^2-n^2 >> kn$, and Taylor expanding the cosine term, derived from the Bessel function expansion, we may set

$$J_{n+k}(r) \cong \left(\frac{2}{\pi}\right)^{1/2}(r^2-\nu^2)^{-1/4}\cos[g(r)-(k-\delta)\xi] \ ,$$

where

$$r = (2nh_1)^{1/2} \quad , \quad \xi = \cos^{-1}(\nu/r) \ ,$$

$$g(r) = (r^2-\nu^2)^{1/2} - \xi - \pi/4 \ , \tag{C3}$$

and all the validity conditions are built into

$$\nu >> 1 \quad , \quad r-\nu >> (\nu/2)^{1/3} \ .$$

A new series of transformations, analogous to the ones performed during the derivation of the map (1) for the uniform $\underset{\sim}{B}$-field case[2] leads to the following Hamiltonian

$$\hat{M} = -\ [\delta_0+\varepsilon n s \sin\Omega\hat{X}_2]\hat{h}_2-\hat{h}_2-A\sum_k \cos[\hat{h}_1 + (\delta-k)\varphi]\sin[\hat{x}_1 + k\hat{x}_2] \ . \tag{C4}$$

Here

$$\delta_0 = \nu-n \ , \tag{C5}$$

$$\hat{h}_1 = (r^2-\nu^2)^{1/2} - \nu\xi - \pi/4 = g[(2nh_1)^{1/2}] \tag{C6}$$

$$\hat{h}_2 = h_2\nu^2\,\frac{(r^2-\nu^2)^{1/2}}{r^2} \ ,$$

$$\hat{X}_1 = n\vartheta_1-\vartheta_2 = X_1 \ , \tag{C7}$$

$$\hat{X}_2 = \vartheta_2/\nu = X_2/\nu \ . \tag{C8}$$

The equation of motion for $\hat{X}_2$ reads $\dot{\hat{X}}_2 = 1$, or equivalently,

$$\vartheta_2 = \nu t \ . \tag{C9}$$

The motion in $\hat{h}_1$, $\hat{x}_1$ plane is given by

$$\begin{aligned} \dot{\hat{x}}_1 &= -\left[\delta_0 + \varepsilon n \sin\Omega t\right] - A \sum_k \sin\left[\hat{h}_1 + (\delta_0 - k)\varphi\right] \sin(\hat{x}_1 + kt) \ , \\ \dot{\hat{h}}_1 &= A \sum_k \cos\left[\hat{h}_1 + (\delta - k)\varphi\right] \cos\left[\hat{x}_1 + kt\right] \ , \end{aligned} \tag{C10}$$

where $A = (2/\pi)^{1/2} \alpha\nu (r^2 - \nu^2)^{1/4}/r^2$ is treated as constant over a finite time period. Now the variables ρ and ϑ are defined through

$$\rho = \hat{h}_1 + \nu\pi \ , \qquad \vartheta = n\pi - \hat{X}_1 \ , \tag{C11}$$

while u and v are introduced as linear combinations of ρ and ϑ according to

$$\dot{u} = \dot{\vartheta} - \dot{\rho} \ , \qquad \dot{v} = \dot{\vartheta} + \dot{\rho} \ . \tag{C12}$$

Combining Eqs. (C11) and (C12) and using the identity

$$\sum_{k=-\infty}^{\infty} \sin(kt) = 2\pi \sum_{j=-\infty}^{\infty} \hat{\delta}(t - 2\pi j) \ ,$$

where $\hat{\delta}$ is the Dirac δ-function, we obtain

$$\dot{u} = \delta(t) - 2\pi A\cos\left[v-(\pi-\xi)\delta_0\right] \sum_{j=-\infty}^{\infty} \hat{\delta}(t-\xi-2\pi j) \ ,$$

$$\dot{v} = \delta(t) + 2\pi A\cos\left[u+(\pi-\xi)\delta_0\right] \sum_{j=-\infty}^{\infty} \hat{\delta}(t-\xi-2\pi j) \ , \tag{C13}$$

with

$$\delta(t) \equiv \delta_0 + \varepsilon n \sin\Omega t \cong \delta_0 + \varepsilon \nu \sin\Omega t \ . \tag{C14}$$

REFERENCES

1. C. F. F. Karney, Phys. Fluids 22, 2188(1979).

2. C. F. F. Karney, Phys. Fluids 21, 1584(1978).

3. T. M. Antonsen, Jr. and E. Ott, Phys. Fluids 24, 1635(1981).

4. S. Riyopoulos, T. M. Antonsen, Jr. and E. Ott, Phys. Fluids, 27, 184(1984).

5. V. I. Arnold, Soviet Math. Dokl. 5, 581(1964).

6. Y. Gell and R. Nakach, Phys. Fluids 23, 1646(1980).

7. A. Deprit, Celestial Mechanics 1, 1(1969).

8. A. Deprit, Celestial Mechanics, 1, 222(1969).

9. V. I. Arnold, "Mathematical Methods of Classical Mechanics", Springer-Verlag, 1978.

10. H. Poincare, "New Methods in Celestial Mechanics", Dover, 1957.

11. J. Ford in "Topics in Non-Linear Dynamics", S. Jorna, editor, (1978).

12. B. V. Chirikov, Phys. Rep. 52, 264(1979).

13. J. M. Green, Ann. N. Y. Acad. Sci. 357, 80(1980).

14. J. P. Codaccioni, F. Doveil and D. F. Escande, Phys. Rev. Lett. 49, 1879(1982).

15. F. Doveil and J. T. Mendonca, Phys. Fluids 26, 3279(1983).

16. B. V. Chirikov, Phys. Reports 52, 265(1979).

17. J. L. Tennyson, M. Month and J. C. Herra (eds.), op cit, p. 158 (1979).

18. S. Riyopoulos, Ph.D Thesis, Chapter XIV.D2, University of Maryland, 1983.

19. J. J. Schuss, T. M. Antonsen, Jr., and M. Porkolab, Nucl. Fusion 23, 201(1983).

20. P. T. Bonoli and E. Ott, Phys. Fluids 25, 359(1982).

21. E. Ott, Phys. Fluids 22, 1739(1979).

22. P. L. Andrews and F. W. Perkins, Phys. Fluids 26, 2537(1983).

23. P. L. Andrews and F. W. Perkins, Phys. Fluids 26, 2546(1983).

FIGURE CAPTIONS

Fig. 1 Surface of section with the $\vartheta_2 = 2\pi$ plane expressed through (a) velocity-like variables Q_y, q_y and (b) action-angle variables I_1', ϑ_1'. (c) is a blow-up of the framed area in (b). Here $\alpha = 0.0498$, $\nu = 20.10023$, $\Omega = 0.01$ and $\varepsilon = 0.055$ implying $M = 10$, $L = 10$, and $\Delta = 0.00023$.

Fig. 2 Surface of section (I_1', ϑ_1') with $\alpha = 0.0498$, $\nu = 20.10$, $\Omega = 0.01$ and $\varepsilon = 0.0055$. Here $\Delta = 0$. Fig. 2(b) is a blow-up of the framed region in 2(a).

Fig. 3 Same as in 1(a), 1(b) but for a uniform magnetic field (ε=0). Note the absence of islands in phase space.

Fig. 4 Surface of section with the same parameters as in 2(a)-2(b), except here $\nu = 20.09$.

Fig. 5 Transition to chaotic behavior. $\nu = 20.10$, $\Omega = 0.01$, $\varepsilon = 0.0055$ and (a) $\alpha = 0.0995$ (b) $\alpha = 0.199$, (c) $\alpha = 0.398$, (d) $\alpha = 1.194$.

Fig. 6 Surface of section showing emergence of second order islands. Here $\alpha = 0.199$, $\nu = 15.575$, $\Omega = 0.01$, $\varepsilon = 0.0055$ implying $M_0 = 31$, $L_0 = 15$.

Fig. 7 Ratio of the stochasticity threshold with frequency modulation A_s' to the constant frequency threshold A_s. Ω is the modulation frequency, $\nu = 21.1$, $\varepsilon = .01$. Bars represent numerical and squares theoretical results respectively.

Fig. 8 Limits of the stochastic regime in the perpendicular velocity space in a uniform magnetic field with $\alpha = 3.382$, $\nu = 30.243$.

Fig. 9 Stochastic regime in the perpendicular velocity space for a large size ripple in the magnetic field. The wave amplitude is the same as in Fig. 8; $\nu = 30.243$, $\varepsilon = 0.3$, $\Omega = 0.01$. Initially, ions start with $v_\perp \cong v_\parallel$. It is evident from Figs. 9(a), 9(b), that the stochastic limits in the velocity space are extended much lower than in Figs. (8a),(8b). Note also from Fig. 9(c), the projection of the surface of section into the P_z, z plane, that some ions gain enough perpendicular velocity to become trapped in the ripple.

Fig. 10 Stochasticity threshold in velocity as a function of ripple size ε. Wave amplitude $\alpha = 3.382$ is well above α_s. Solid line is the theoretical prediction. Velocity v in the perpendicular axis is normalized according to $v = v_\perp k_\perp/\omega_c$.

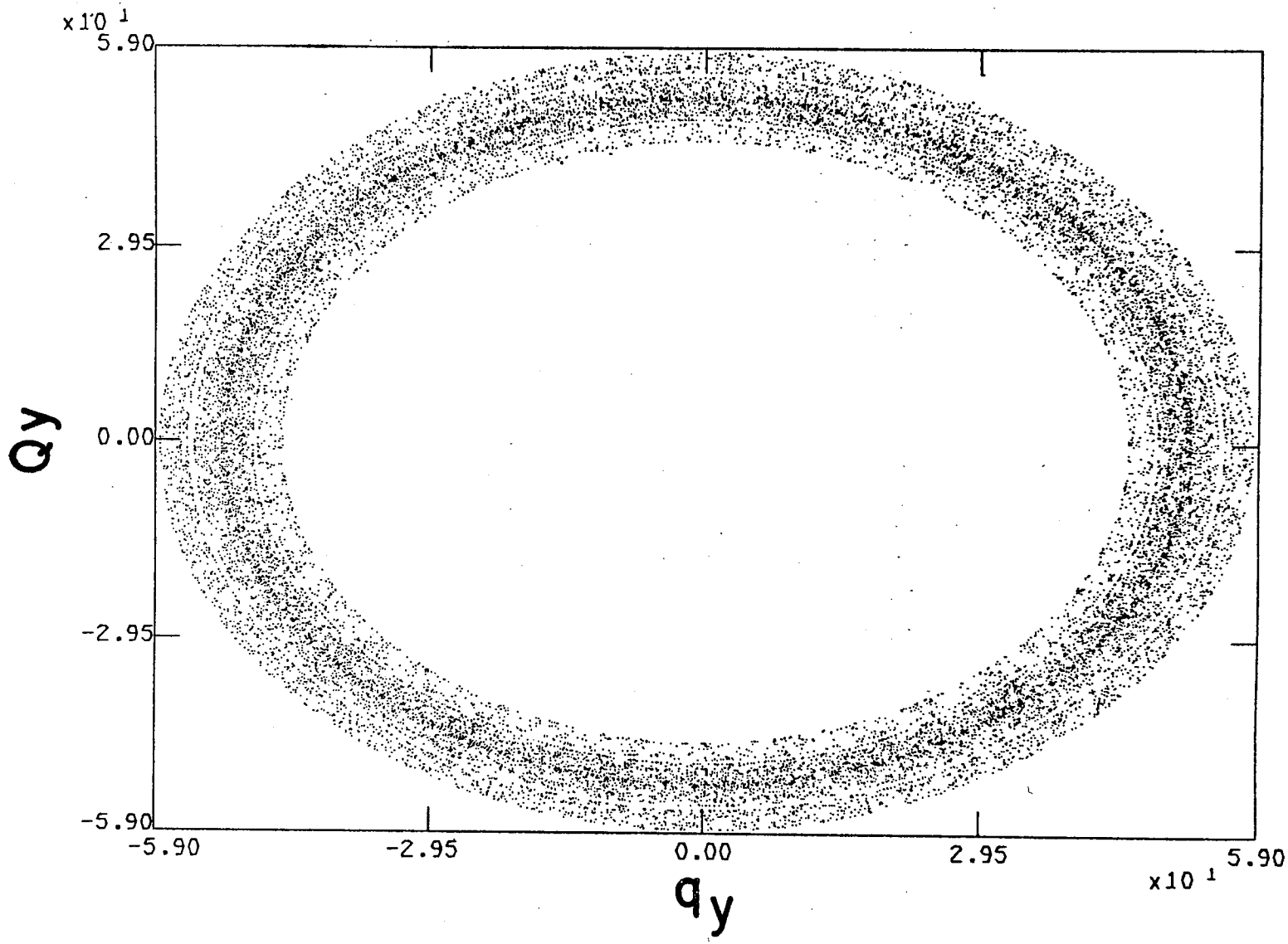

FIG. 1a

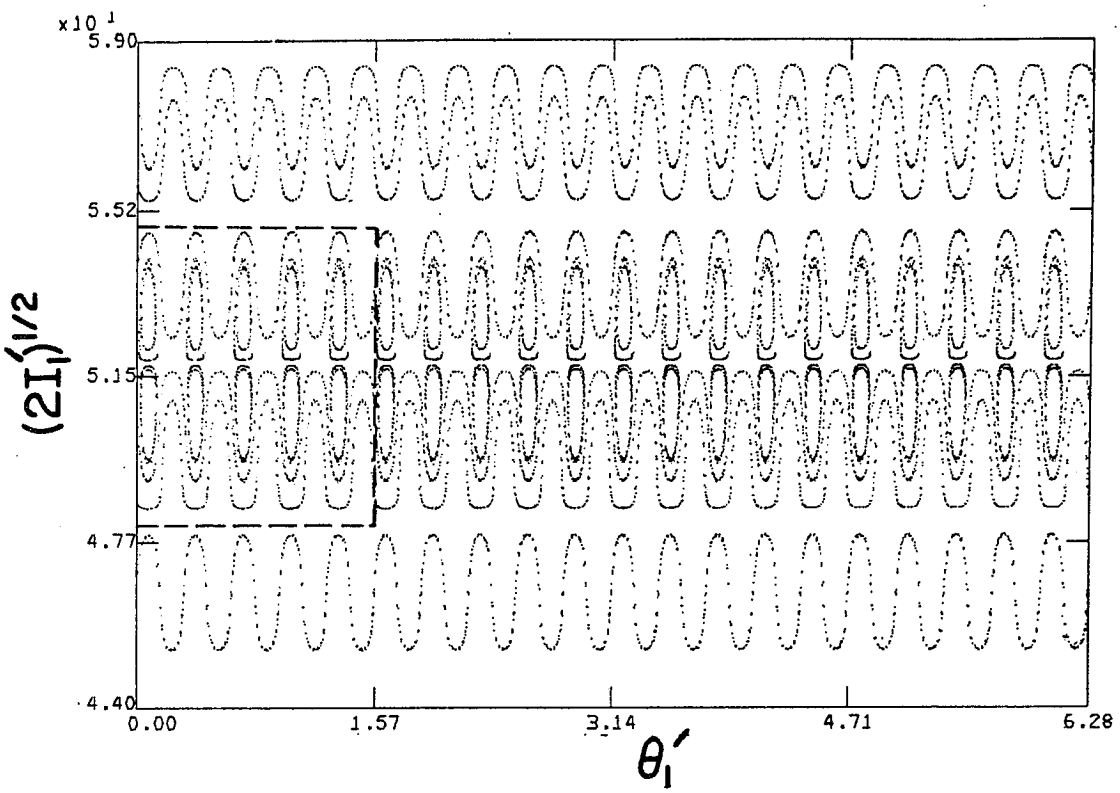
x10 1
5.90
5.52
5.15
4.77
4.40
0.00
1.57
3.14
4.71
6.28
$(2I_1')^{1/2}$
θ_1'

FIG. 1b

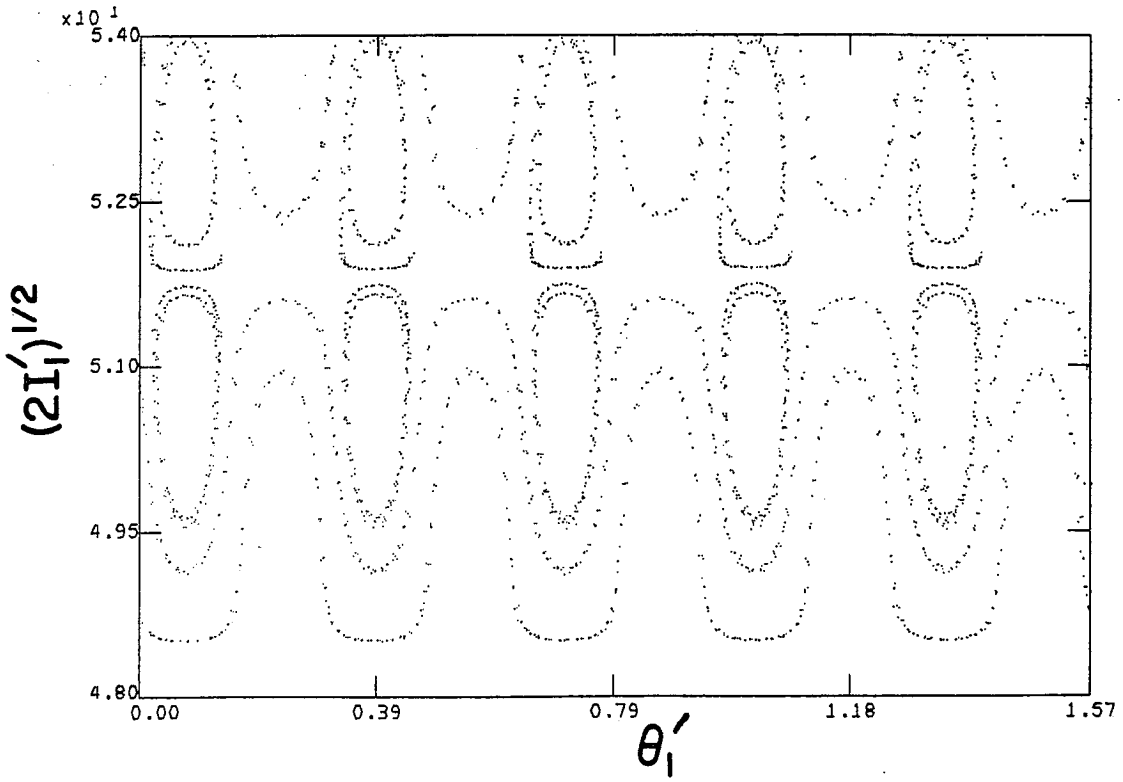
x10 1
5.40
5.25
5.10
4.95
4.80
0.00
0.39
0.79
1.18
1.57
$(2I_1')^{1/2}$
θ_1'

FIG. 1c

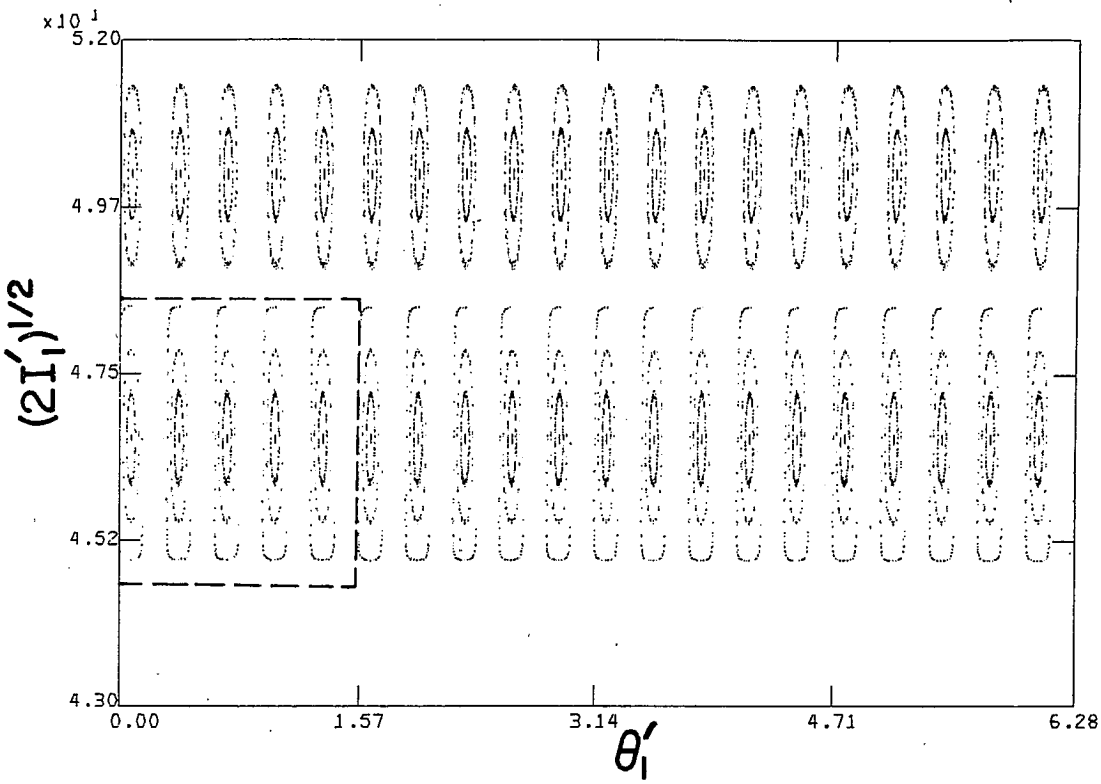
x10 1
5.20
4.97
4.75
4.52
4.30
0.00
1.57
3.14
4.71
6.28
$(2I_1')^{1/2}$
θ_1'

FIG. 2a

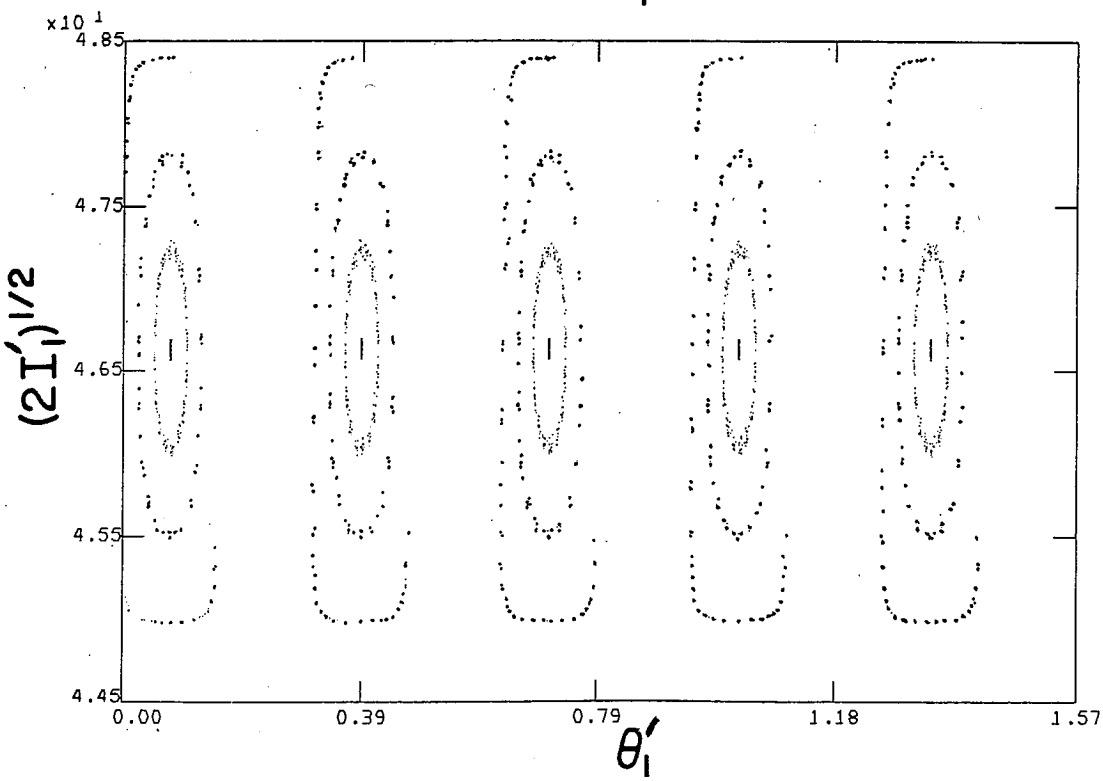
x10 1
4.85
4.75
4.65
4.55
4.45
0.00
0.39
0.79
1.18
1.57
$(2I_1')^{1/2}$
θ_1'

FIG. 2b

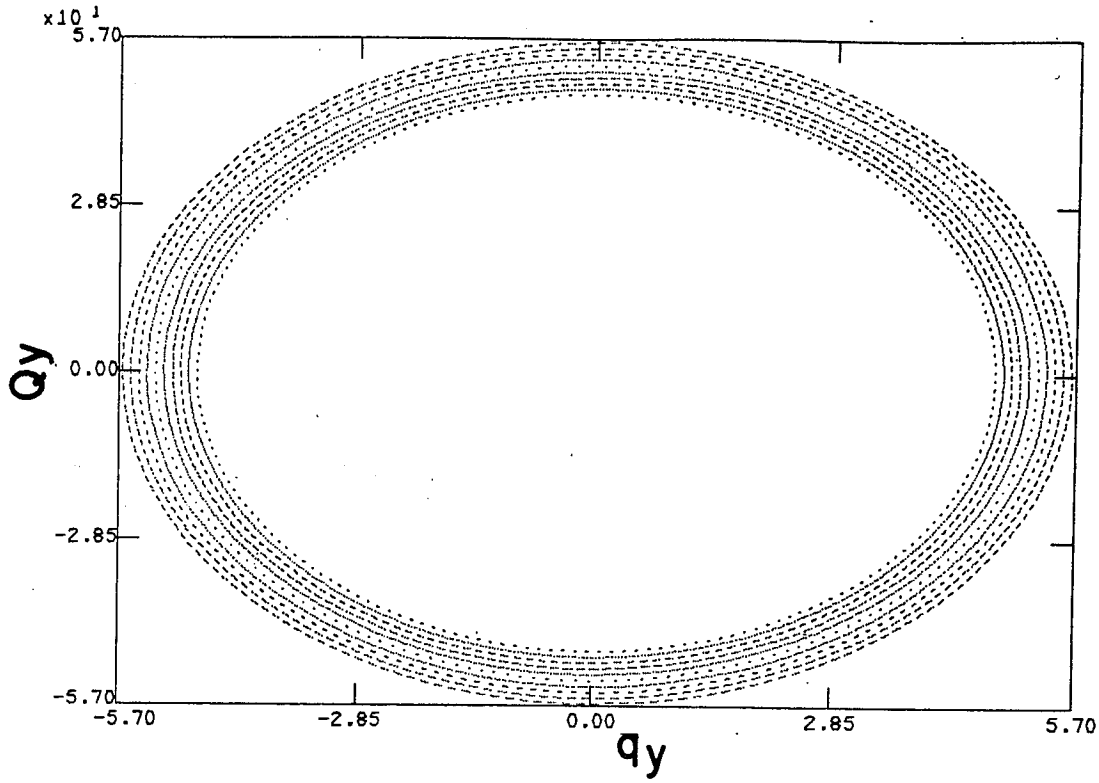
x10 1
5.70
2.85
0.00
-2.85
-5.70
Qy
-5.70
-2.85
0.00
2.85
5.70
qy

FIG. 3a

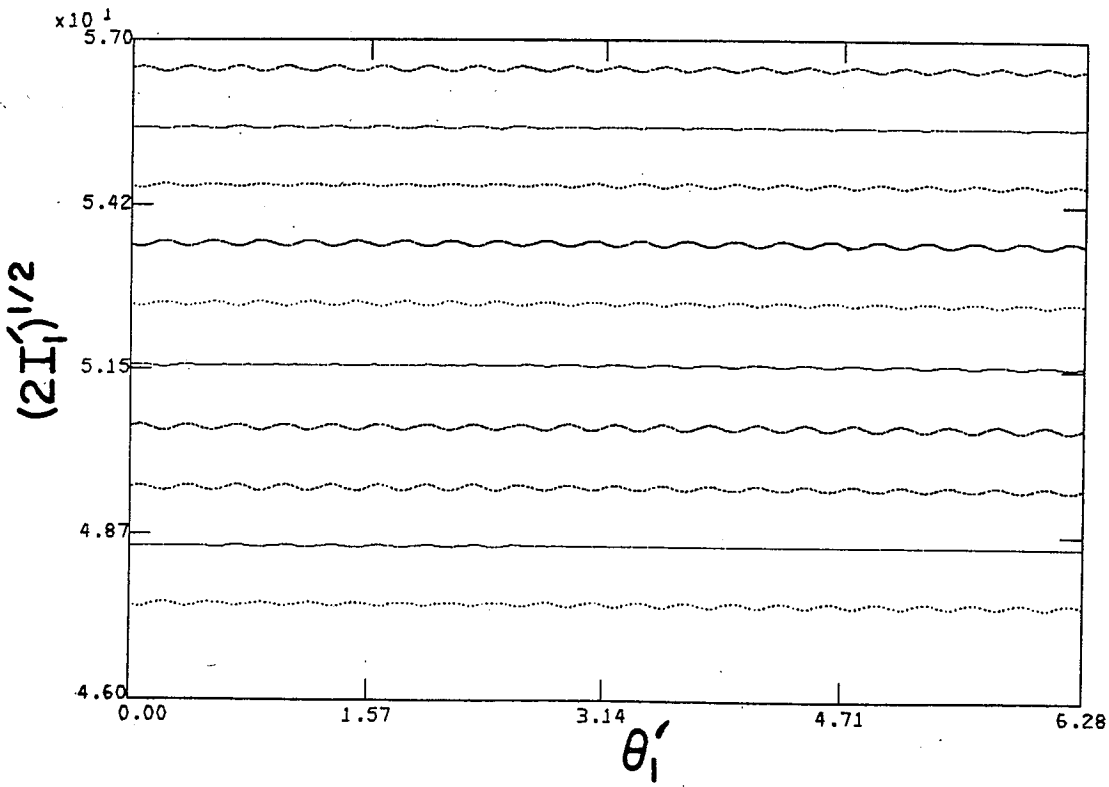
x10 1
5.70
5.42
5.15
4.87
4.60
$(2I_1')^{1/2}$
0.00
1.57
3.14
4.71
6.28
θ_1'

FIG. 3b

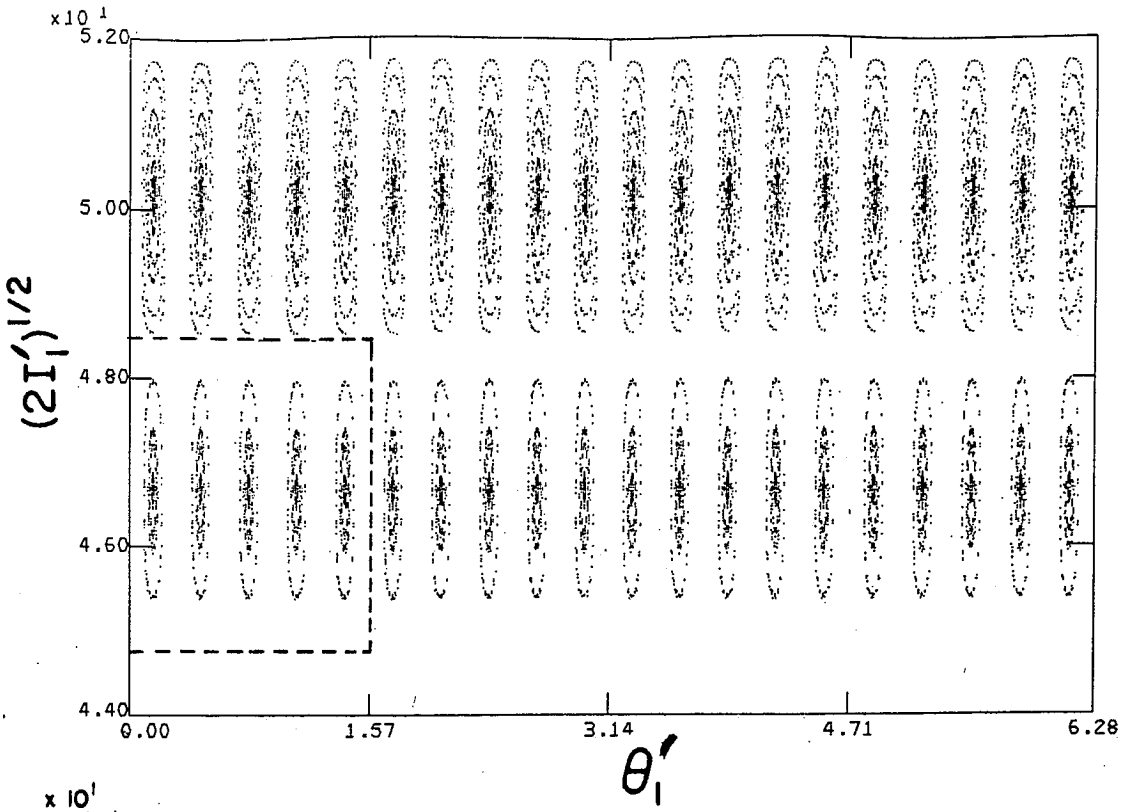
x10 1
5.20
5.00
4.80
4.60
4.40
$(2I_1')^{1/2}$
0.00
1.57
3.14
4.71
6.28
θ_1'

FIG. 4a

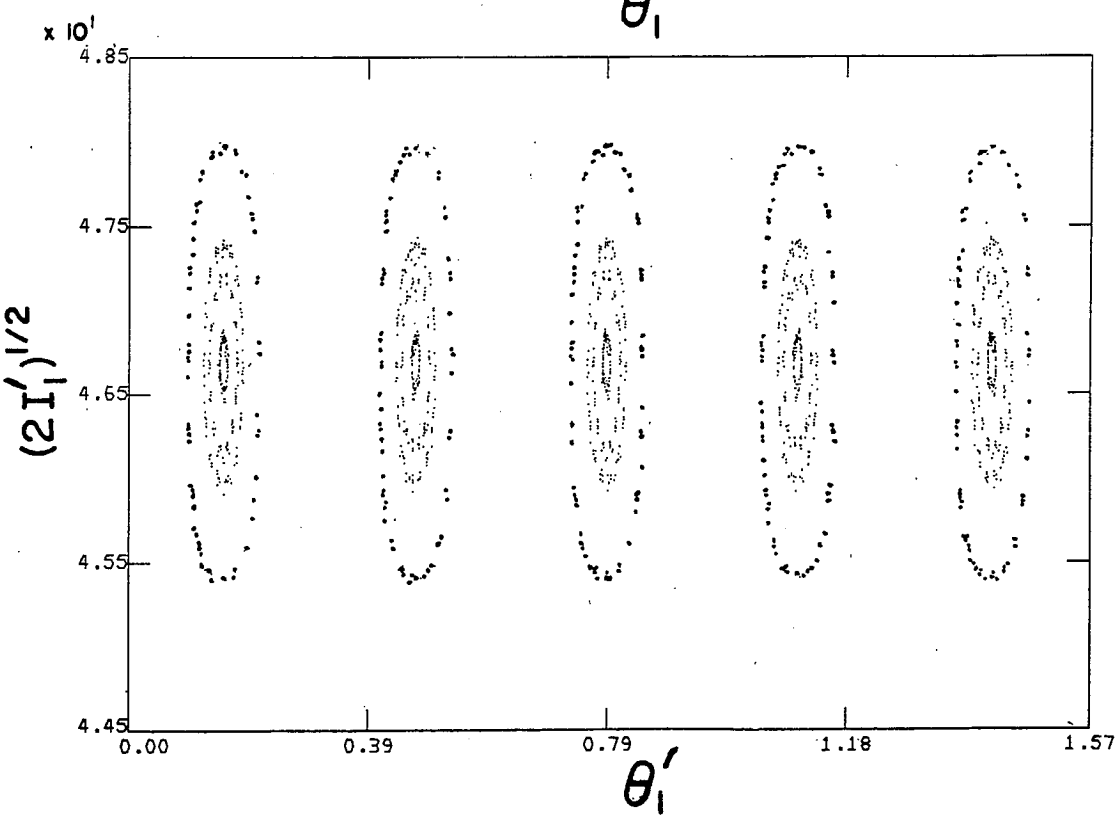
x 10'
4.85
4.75
4.65
4.55
4.45
$(2I_1')^{1/2}$
0.00
0.39
0.79
1.18
1.57
θ_1'

FIG. 4b

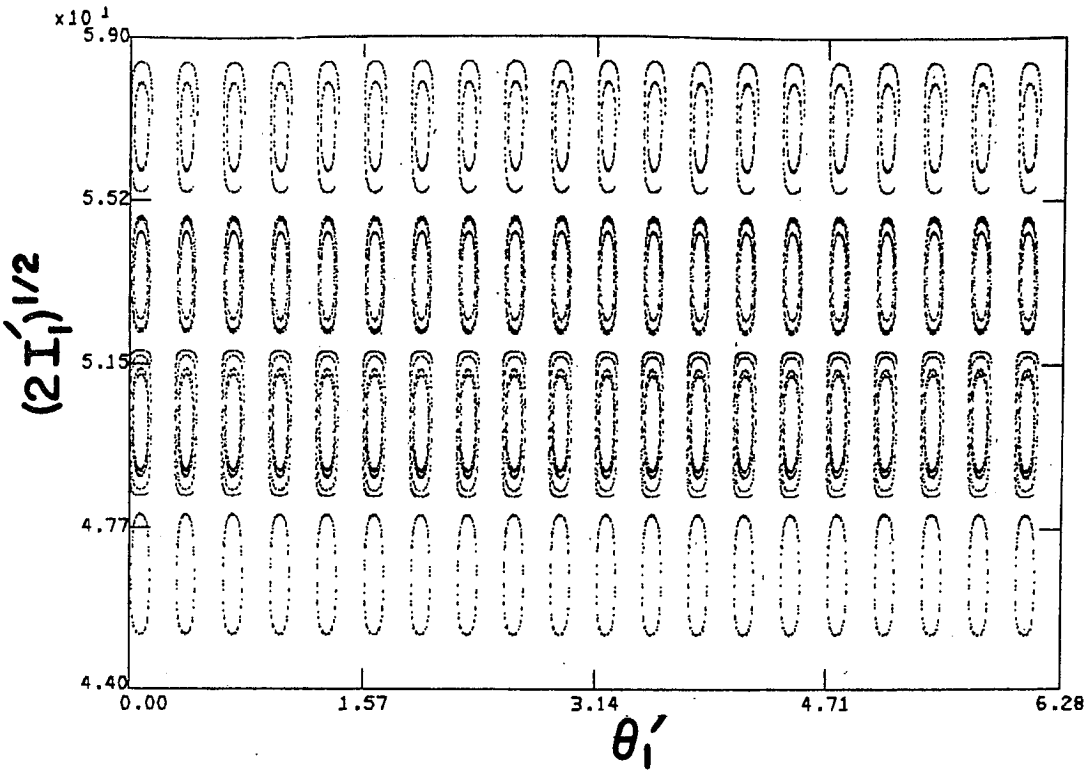
x10 1
5.90
5.52
5.15
4.77
4.40
0.00
1.57
3.14
4.71
6.28
$(2I_1')^{1/2}$
θ_1'

FIG. 5a

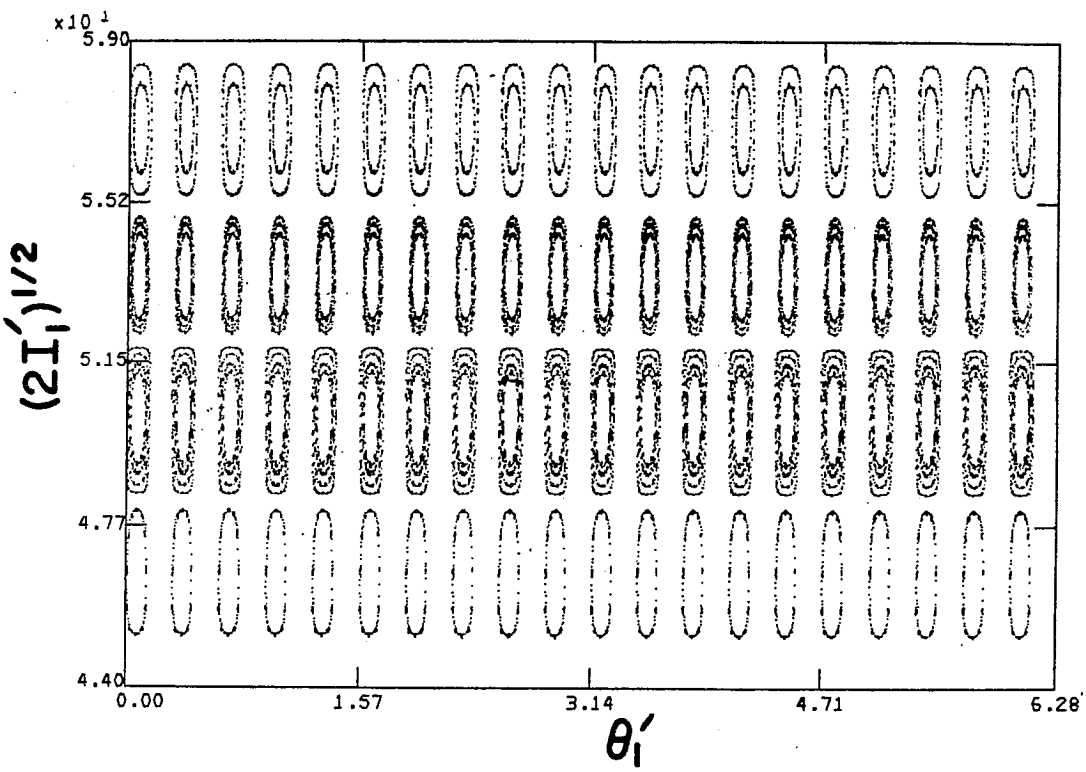
x10 1
5.90
5.52
5.15
4.77
4.40
0.00
1.57
3.14
4.71
6.28
$(2I_1')^{1/2}$
θ_1'

FIG. 5b

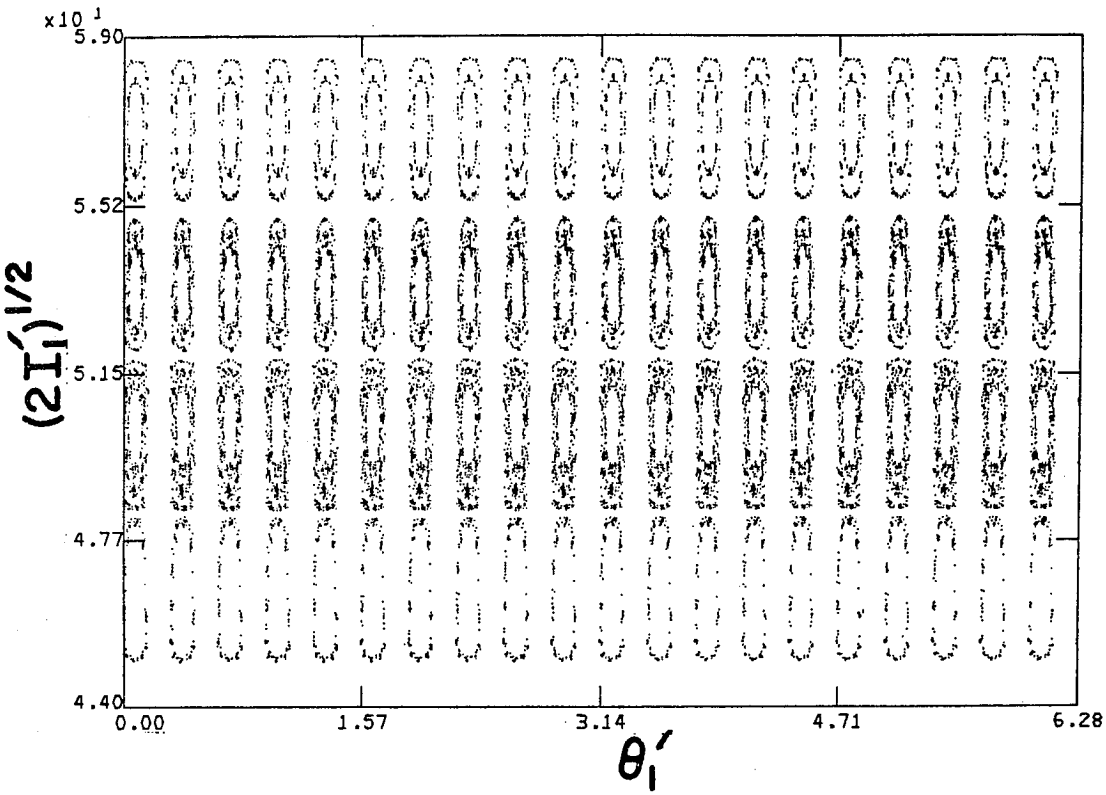
x10 1
5.90
5.52
5.15
4.77
4.40
0.00
1.57
3.14
4.71
6.28
$(2I_1')^{1/2}$
θ_1'

FIG. 5c

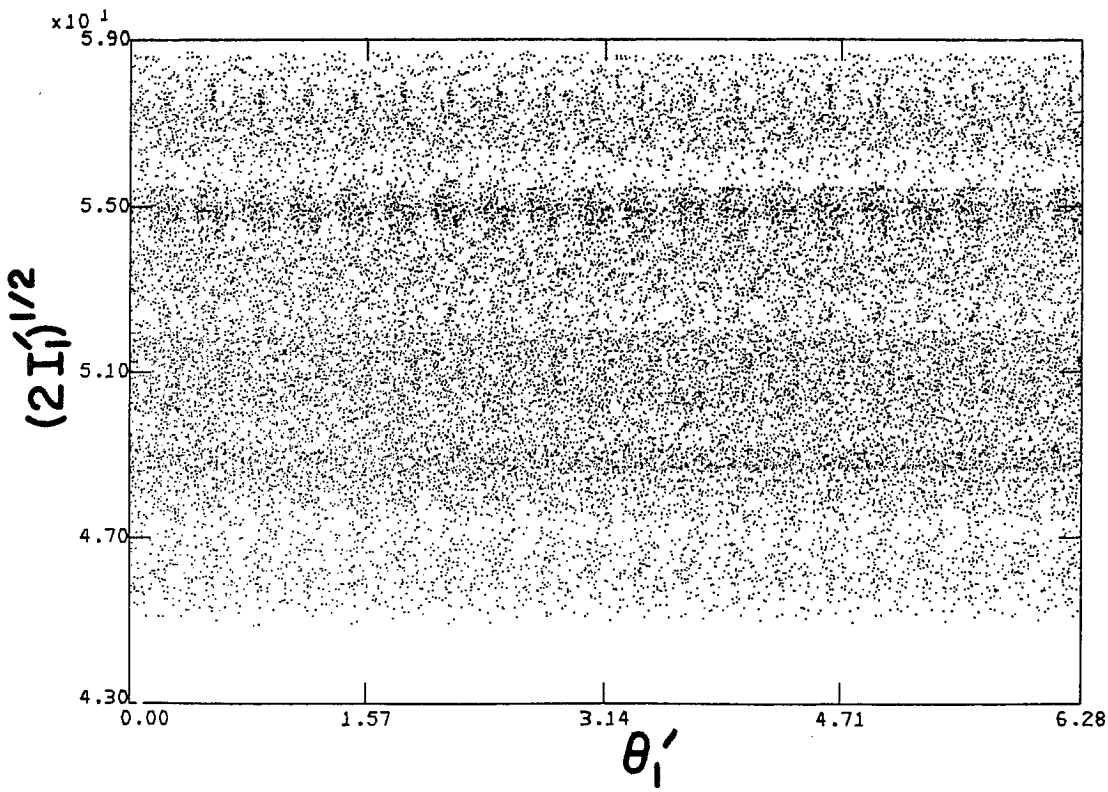
x10 1
5.90
5.50
5.10
4.70
4.30
0.00
1.57
3.14
4.71
6.28
$(2I_1')^{1/2}$
θ_1'

FIG. 5d

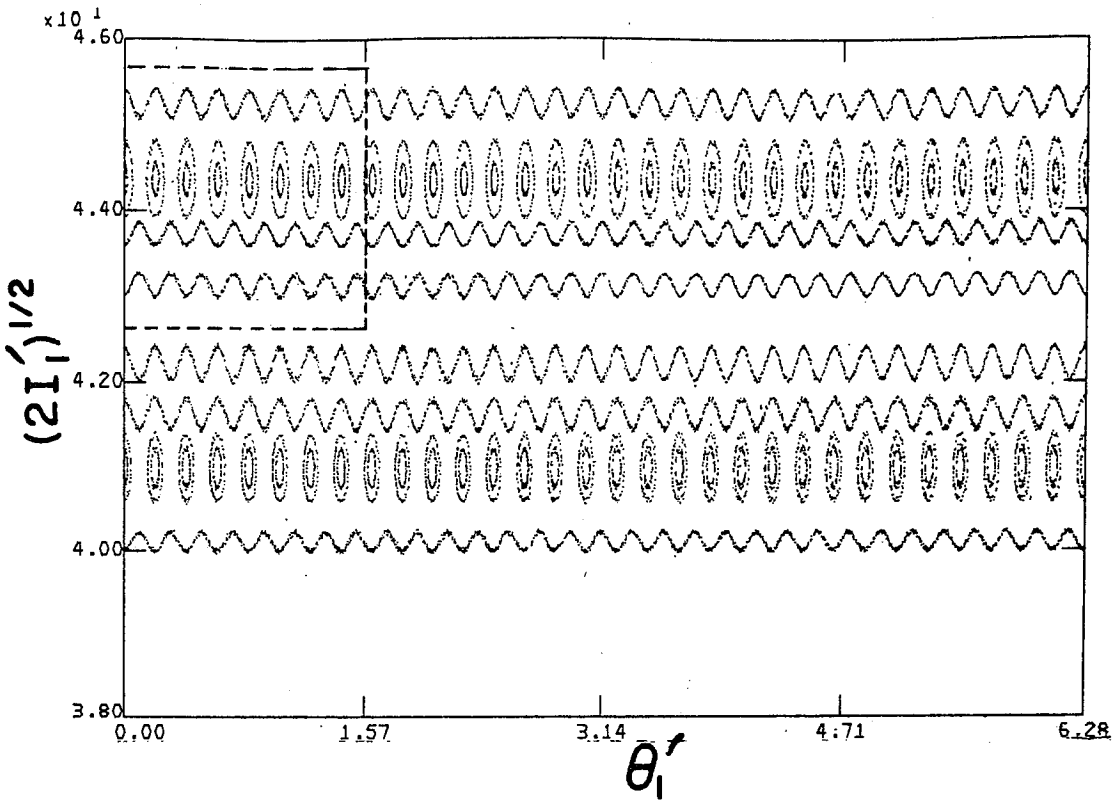
x10 1
4.60
4.40
4.20
4.00
3.80
$(2I_1')^{1/2}$
0.00
1.57
3.14
4.71
6.28
θ_1'

FIG. 6a

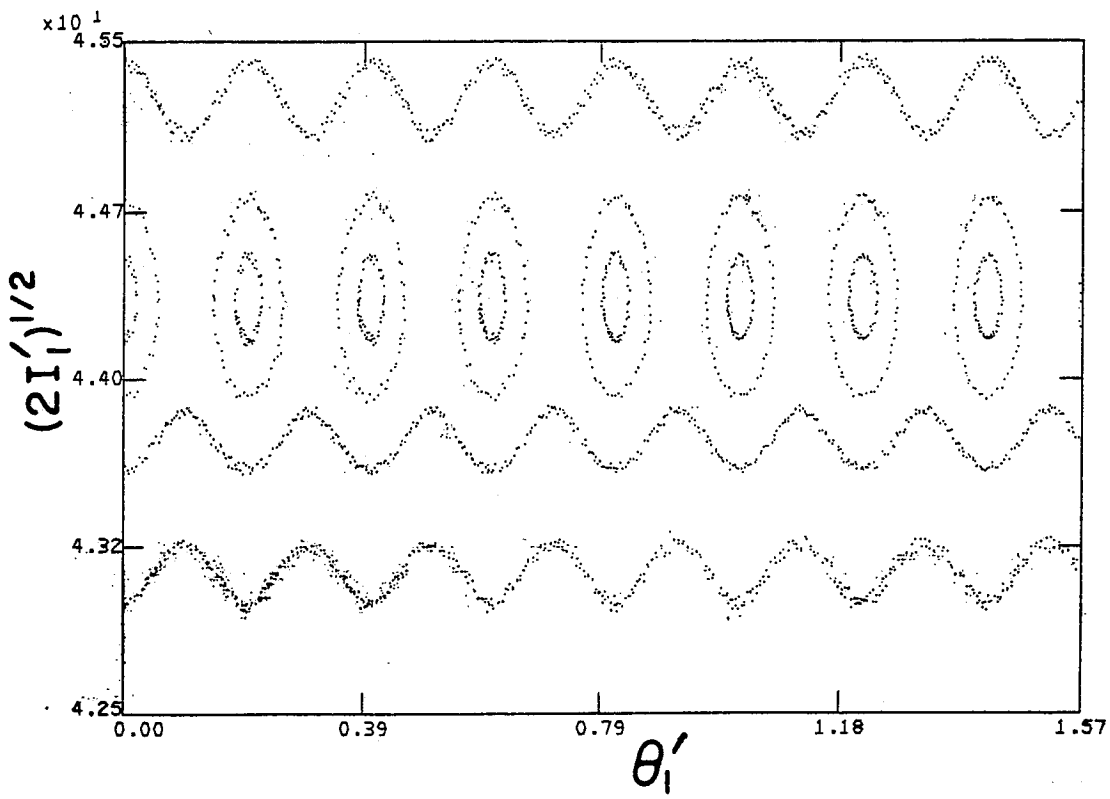
x10 1
4.55
4.47
4.40
4.32
4.25
$(2I_1')^{1/2}$
0.00
0.39
0.79
1.18
1.57
θ_1'

FIG. 6b

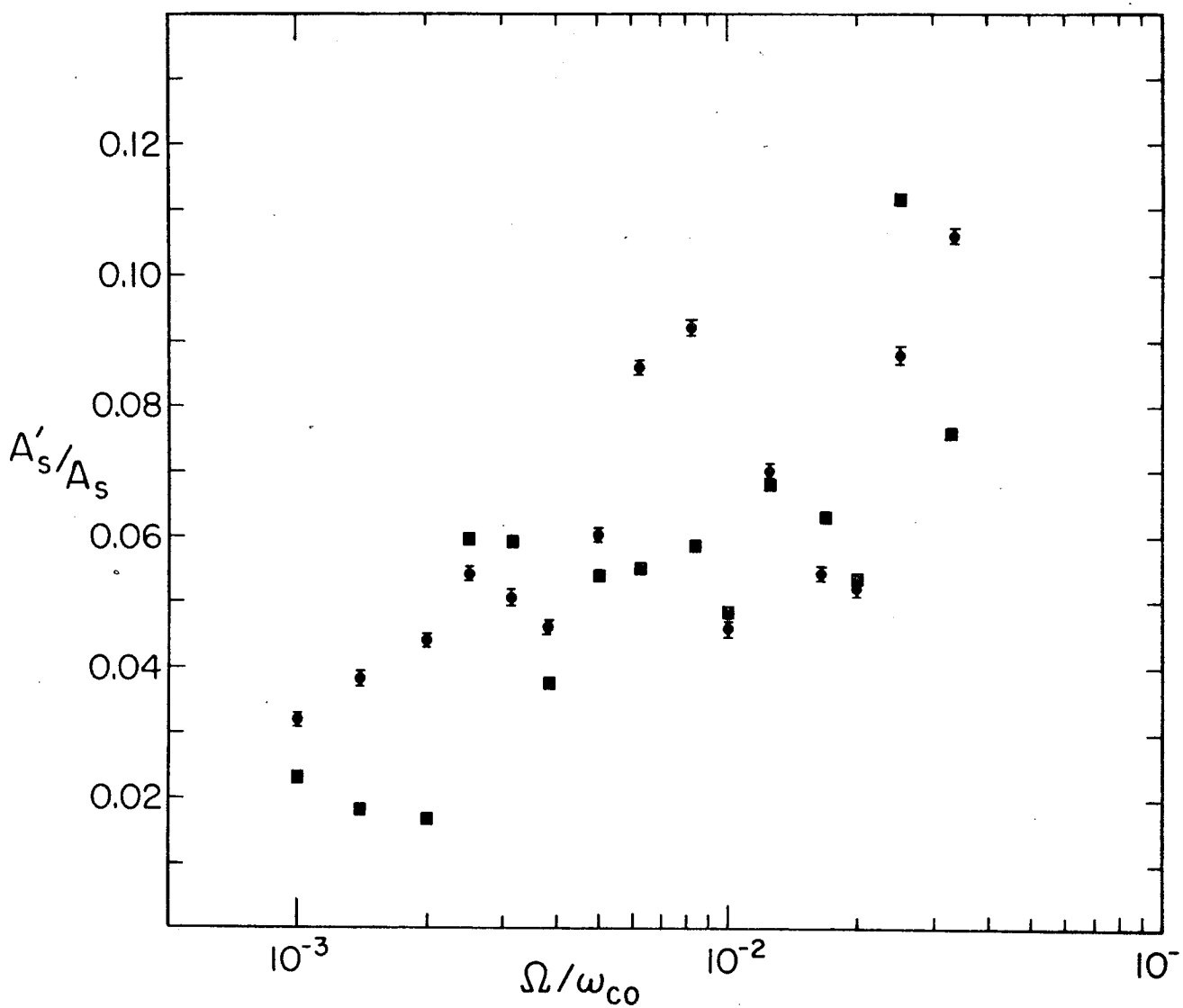

FIG. 7

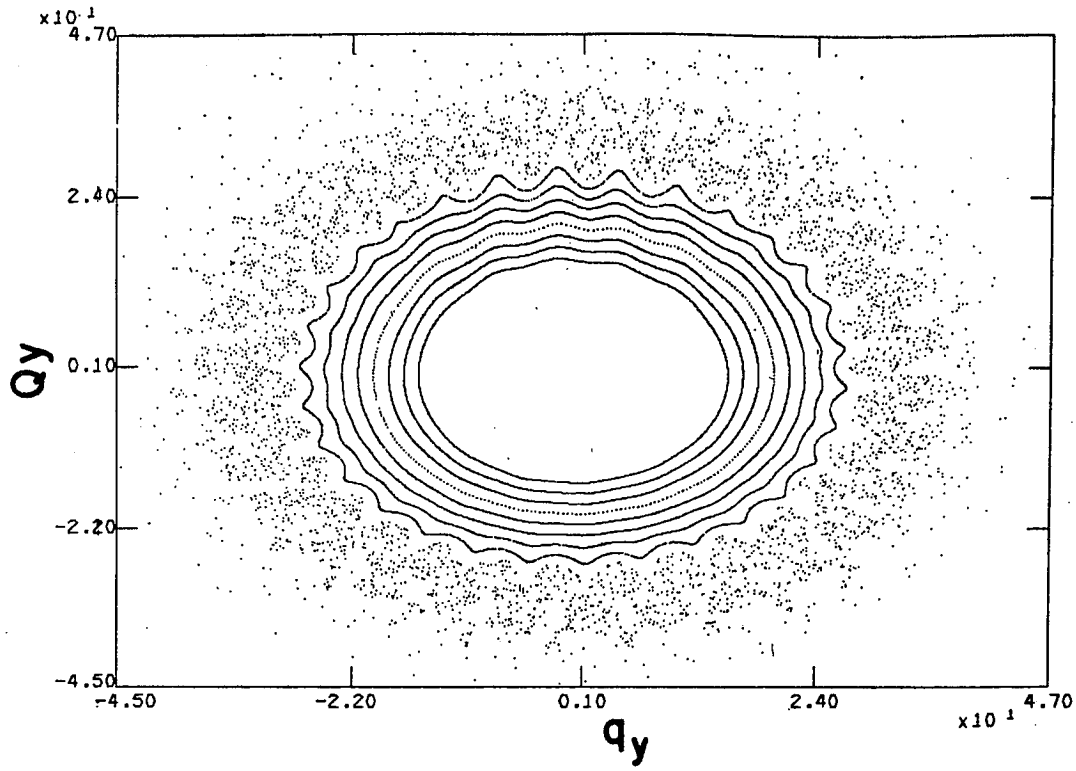
x10 1
4.70
2.40
0.10
-2.20
-4.50
Qy
-4.50
-2.20
0.10
2.40
4.70
x10 1
qy

FIG. 8a

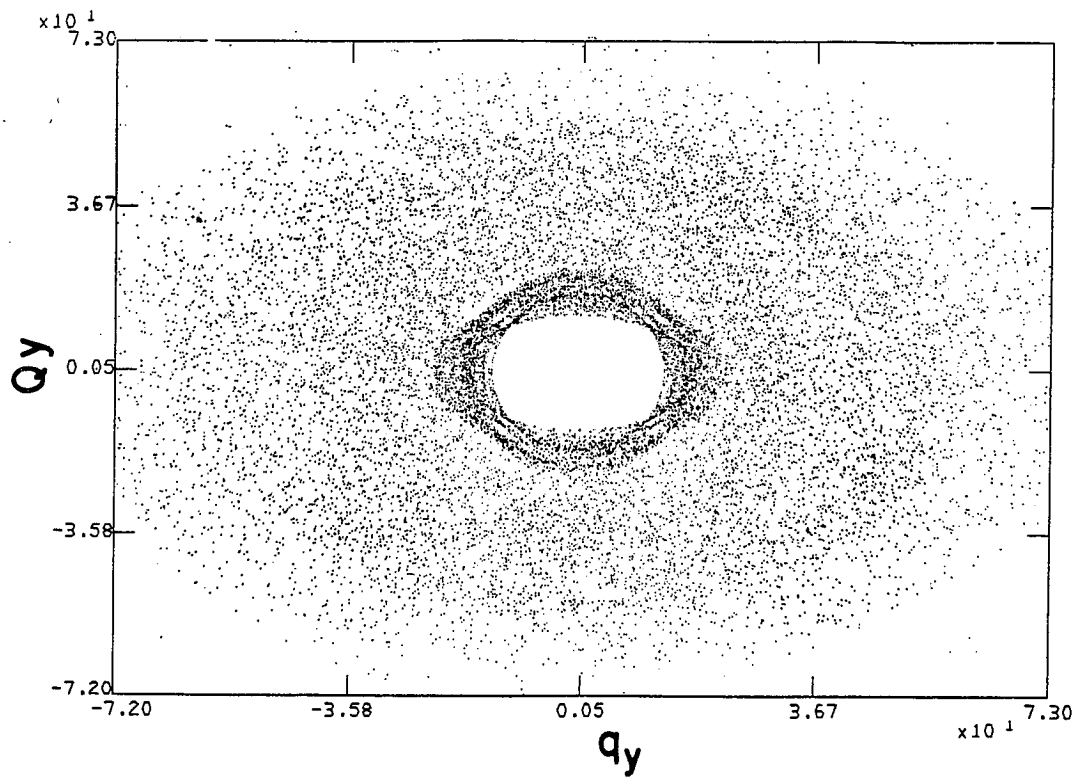
x10 1
7.30
3.67
0.05
-3.58
-7.20
Qy
-7.20
-3.58
0.05
3.67
7.30
x10 1
qy

FIG. 9a

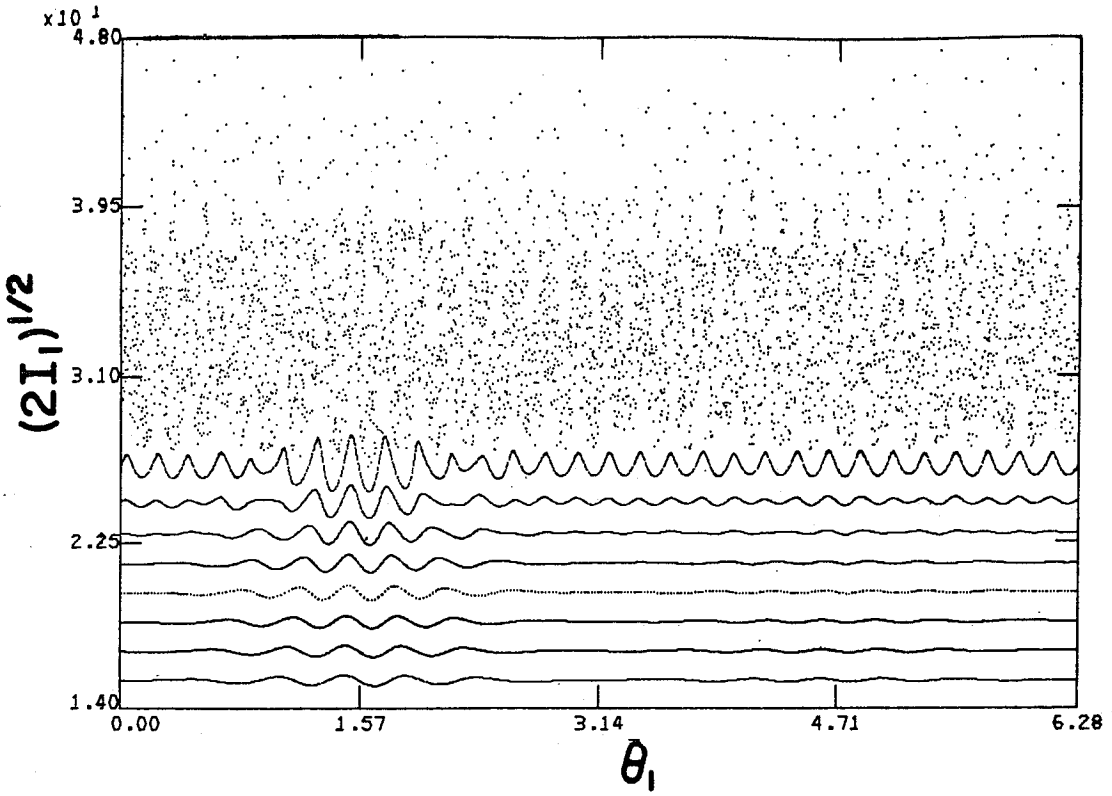
x10 1
4.80
3.95
3.10
2.25
1.40
0.00
1.57
3.14
4.71
6.28
$(2I_1)^{1/2}$
θ_1

FIG. 8b

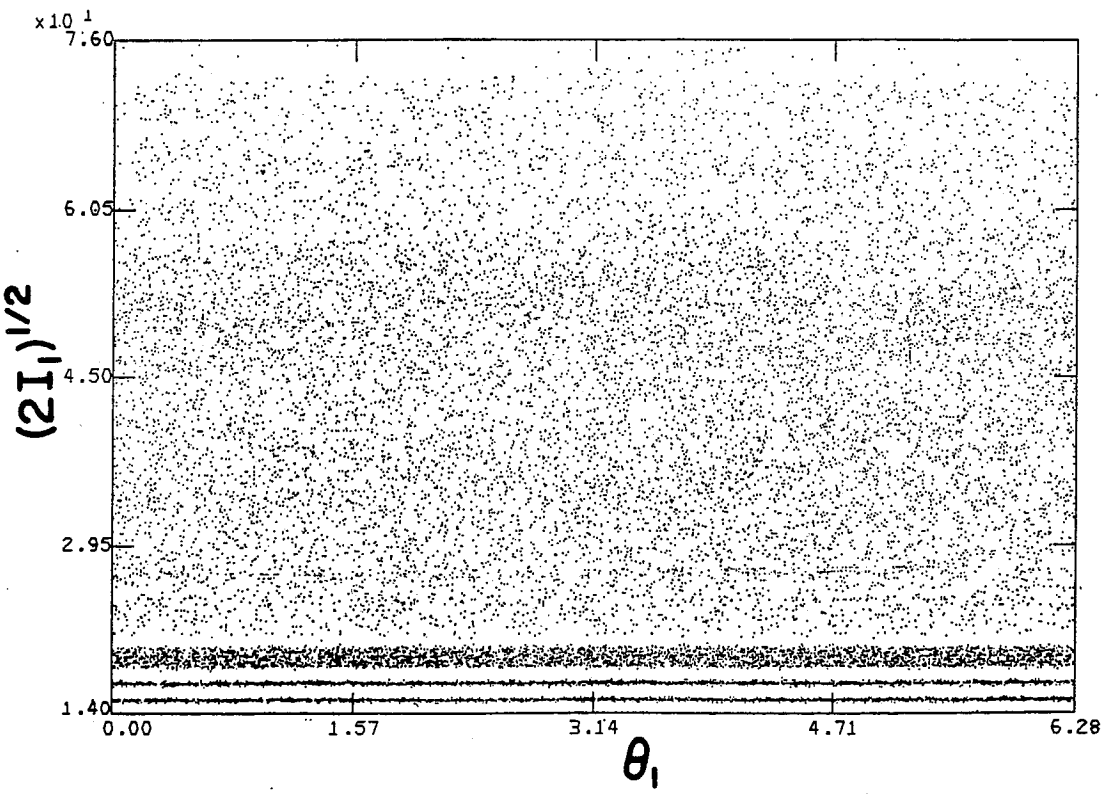
x10 1
7.60
6.05
4.50
2.95
1.40
0.00
1.57
3.14
4.71
6.28
$(2I_1)^{1/2}$
θ_1

FIG. 9b

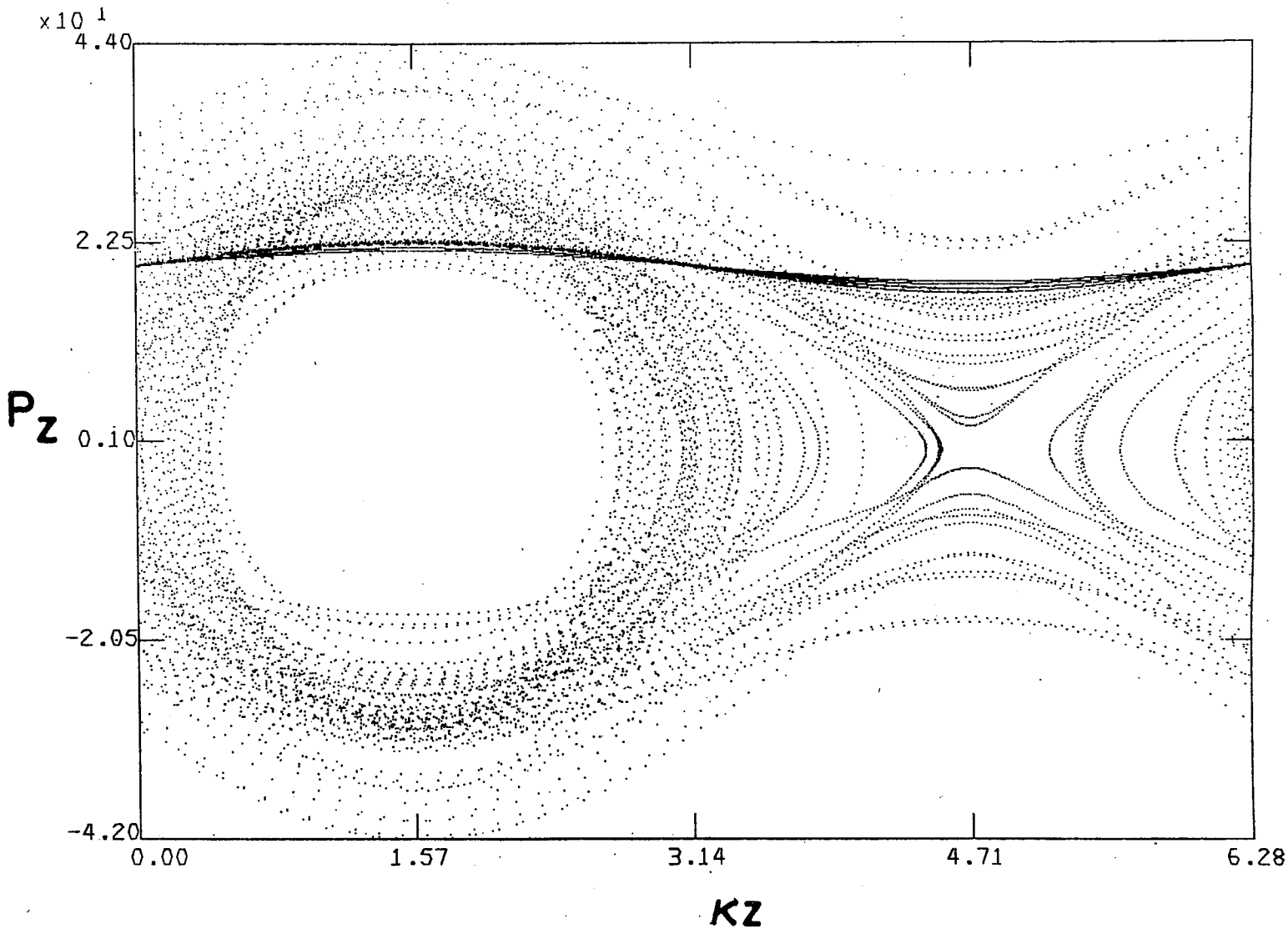

FIG. 9c

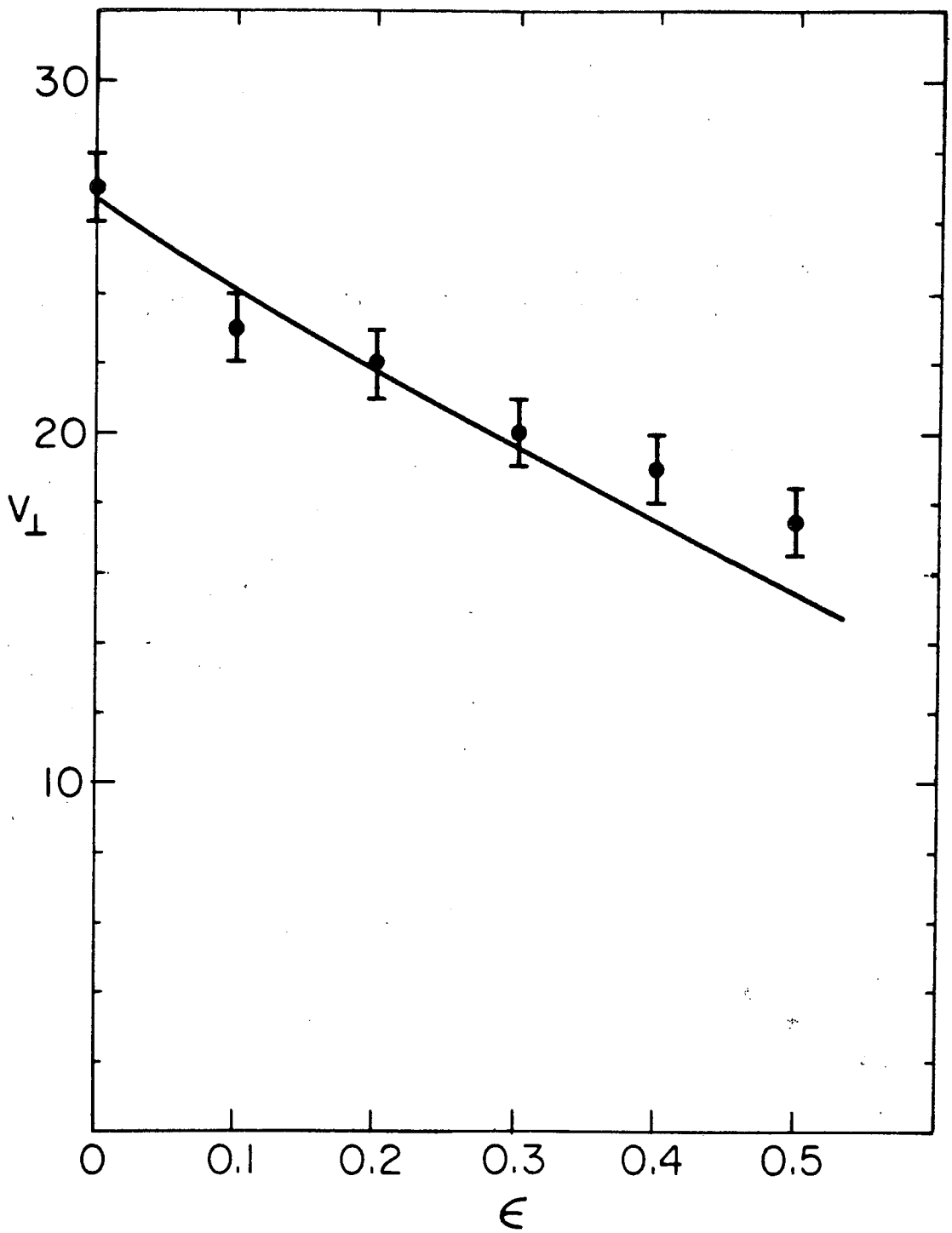

FIG. 10